



Organization of the cytokeratin network in an epithelial cell

Stéphanie Portet^{a,*}, Ovide Arino^b, Jany Vassy^a, Damien Schoëvaert^a

^aLaboratoire d'Analyse d'Images en Pathologie Cellulaire, Institut Universitaire d'Hématologie, Hôpital Saint Louis, 1 Avenue Claude Vellefaux, 75475 Paris Cedex 10, France

^bIRD, UR GEODES, Centre de Bondy, 32 Avenue Henri Varagnat, 93143 Bondy, France

Received 16 July 2001; received in revised form 15 January 2003; accepted 27 February 2003

Abstract

The cytoskeleton is a dynamic three-dimensional structure mainly located in the cytoplasm. It is involved in many cell functions such as mechanical signal transduction and maintenance of cell integrity. Among the three cytoskeletal components, intermediate filaments (the cytokeratin in epithelial cells) are the best candidates for this mechanical role. A model of the establishment of the cytokeratin network of an epithelial cell is proposed to study the dependence of its structural organization on extracellular mechanical environment. To implicitly describe the latter and its effects on the intracellular domain, we use mechanically regulated protein synthesis. Our model is a hybrid of a partial differential equation of parabolic type, governing the evolution of the concentration of cytokeratin, and a set of stochastic differential equations describing the dynamics of filaments. Each filament is described by a stochastic differential equation that reflects both the local interactions with the environment and the non-local interactions via the past history of the filament. A three-dimensional simulation model is derived from this mathematical model. This simulation model is then used to obtain examples of cytokeratin network architectures under given mechanical conditions, and to study the influence of several parameters.

© 2003 Elsevier Ltd. All rights reserved.

Keywords: Cytoskeleton; Intermediate filaments; Organization model; Aggregation model

1. Introduction

The cytoskeleton is composed of three types of filaments (microtubules, *MT*, microfilaments, *MF* and intermediate filaments, *IF*). They are organized as networks, each having different functions and different architectures.

Modeling of the cytoskeleton (re)organization and more generally network organization of a variety of biochemical species and living organisms has attracted the attention of several authors in the recent past. Models of network structures whose architectures depend on their environment have been developed. These models are concerned with angiogenesis processes (Stokes and Lauffenburger, 1991), plant roots (Mech and Prusinkiewicz, 1996), neural networks (Vaario et al., 1997), extracellular matrix fibers (Dallon et al., 1999; Dallon and Sherratt, 2000) as well as with intracellular

actin filaments (Sherratt and Lewis, 1993). Several models have been developed to study the dynamics of the *MF* and *MT* networks using molecular mechanisms (Robert et al., 1990; Dufort and Lumsden, 1993; Civelekoglu and Edelstein-Keshet, 1994; Bolterauer et al., 1996; Mogilner and Edelstein-Keshet, 1996; Spiros and Edelstein-Keshet, 1998; Janosi et al., 1998; Mogilner and Oster, 1999; Sept et al., 1999; Edelstein-Keshet and Ermentrout, 2000). Some of the models using a molecular approach have been extended in order to account for the effects of the extracellular environment on the dynamics of cytoskeleton reorganization (Suci et al., 1997; Wang, 2000). Moreover, a structural approach based on the tensegrity concept (Ingber, 1993) proposes the modeling of the global behavior of the cytoskeleton (Wendling et al., 1999). As far as we know, no such model has ever been proposed for *IF* organization.

The scaffolding of *IFs* generally forms a mesh (● in Fig. 1) which encloses and maintains the position of the nucleus (Goldman et al., 1996). From this perinuclear mesh, *IFs* radiate through the cytoplasm to anchorage regions of the cell membrane (■ in Fig. 1) forming a

*Corresponding author. Department of Physics, P412 Avadh Bhatia, University of Alberta, Edmonton, Alberta, Canada T6G 2J1. Tel.: +1-780-492-1064; fax: +1-780-492-0714.

E-mail address: sportet@phys.ualberta.ca (S. Portet).

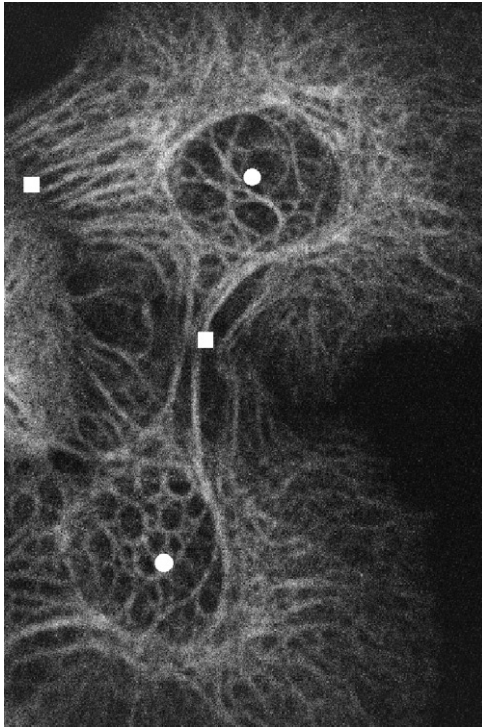


Fig. 1. *CK* networks of cells, imaged by immunofluorescence and confocal microscopy. Regions marked by ■ are desmosome plaques, the cell–cell junction areas. Regions marked by ● are the perinuclear regions surrounding the cell nuclei: *CK* filaments cover the surfaces of nuclei. The image was provided by Jany Vassy.

link between the extracellular environment and the nucleus. The *IF* network exhibits different architectural patterns depending on intracellular locations (Portet et al., 1999) corresponding to specific strain regions in the cell. *IFs* also have specific rheological properties (Ma et al., 1999); they resist high strain by increasing their stiffness (Wang and Stamenovic, 2000).

The soluble subunits of *IFs*, the *tetramers*, are fibrous proteins consisting of two coiled coils (Geisler et al., 1998). Tetramers, also called the *soluble pool* (Hatzfeld and Burba, 1994), are the building blocks of *IFs*. Eight tetramers aggregate laterally to form a unit-length filament (*ULF*). *ULFs* anneal longitudinally to yield filaments (Herrmann and Aebi, 2000). As subunits of filaments, they are fixed and form what is called the *insoluble pool*.

The *IF* network plays a mechanical role (Eckes et al., 1998; Chou and Goldman, 2000; Coulombe et al., 2000). It can reorganize its architecture in response to modifications of the extracellular environment (Wang and Ingber, 1994; Thoumine et al., 1995): in this way, it might mediate mechanical signals from the extracellular environment to the nucleus (Ingber, 1997). It could also preserve what is known as cell integrity (Sarria et al., 1994). The aim of our work is to study, by means of a model, the dependence of the structural organization of the *IF* network on its mechanical environment,

implicitly described by a mechanically regulated protein synthesis (Chicurel et al., 1998). We focus on cytokeratins (*CK*), the major protein components of *IFs* expressed in epithelial cells (Bray, 1992). Thus, our model describes the establishment of the *CK* network in an epithelial cell, driven by mechanical conditions by accounting for

- the (phenomenological description of the) mechanical environment and its effects on the intracellular domain,
- and the building up of filaments by partial aggregation of the *CK*.

It is assumed that the mechanical environment regulates *CK* synthesis, which we assume to take place at strain regions in the cytoplasm, with rates depending on the nature of the strain. The action of the mechanical environment is modeled without explicit reference to either the nature of the signal or the detailed description of the mechanisms. Each filament is the material trajectory of a solution of a stochastic differential equation (SDE) whose coefficients reflect both the local interactions with the environment via the concentration gradient, and the non-local interactions via the past history of the filament. Thus the model is a hybrid of a partial differential equation (PDE) of parabolic type, governing the evolution of the concentration of *CK*, and a set of SDEs describing the dynamics of filaments. A numerical code has been implemented for the model and a number of virtual experiments have been performed. A typical experiment shows the building up of filaments and their progression from the source sites through the cytoplasm; as time goes on, more and more filaments are produced, until the emergent network stabilizes. As a first attempt to quantify these results, some features have been extracted to ascertain to what extent the density of the network or the shape of the filaments is influenced by either diffusion, stochastic terms or the initial conditions of the SDE. Our analysis is strictly numerical we do not attempt a rigorous analytic treatment.

The paper is organized as follows: Section 2 is devoted to modeling concepts; in Section 3, the components of the mathematical model are explained in detail, and the general equations are stated. In Section 4, results of numerical experiments are presented. Finally, Section 5 provides a general discussion of the model and the numerical results. Details about numerical computations are deferred to Appendix A.

2. Modeling concepts

At the end of mitosis, once the telophase step has been completed, the cell divides into two daughter cells (*cytodieresis*), and the nuclear envelope is formed. The

present work models the establishment of the *CK* network from this time (henceforth denoted as the *initial time* $T_0 = 0$ of the model) onwards. The temporal domain is $[0, T_{max}]$, where T_{max} is the cell doubling time. The spatial domain is the region defined by a cell, made up of a cellular membrane, a cytoplasm, a nucleus and its nuclear envelope. Moreover, we consider epithelial cells, where a basal-apical polarity divides the membrane into three domains: the basal surface in contact with the extracellular matrix (ECM), the lateral surfaces in contact with the adjacent cells and the apical surface in contact with the lumen (Bray, 1992).

2.1. Extracellular mechanical environment and its effects on the intracellular domain

Immediately following the end of cytodieresis, it is hypothesized that a centripetal field of forces is established around the nucleus, as a body force responsible for maintaining nuclear integrity. After a while, the cell differentiates into an epithelial cell. It then anchors to the ECM via *hemidesmosomes* and adheres to other adjacent epithelial cells via *desmosomes*. The hemidesmosomes, containing integrins, are located at the basal surface (Sonnenberg et al., 1993), and the desmosomes, containing cadherin-family members, form plaques several microns in diameter on the lateral surfaces of the cells (Fig. 1) (Smith and Fuchs, 1998). The extracellular mechanical environment acting on the cell is then assumed to be composed of tension or/and pressure caused by the two types of junctions, the hemidesmosomes and the desmosomes.

The type of strain determines where it will act spatially and when it will be activated. Cohesion forces, which preserve the nuclear integrity and act at the perinuclear region, are postulated to be active at the initial time. Strain resulting from junctions, acting on hemidesmosomes and on desmosomes respectively, is assumed to be initiated in sequence after the onset of cell differentiation.

Our main working hypothesis is that *the action of mechanical strain triggers and regulates the synthesis of cytoskeletal proteins*. Motivated by the observations of Chicurel et al. (1998) in the case of focal adhesion complexes, when mechanical strain is applied to the cell (step (1) in Fig. 2(a)), we assume that it reacts by relocating the synthesis of *CK* proteins to the regions surrounding the strain in order to build a network capable of preserving its integrity (step (2) in Fig. 2(a)). In other words, we assume that mechanical stress induces the transport of ribosomes and messenger RNAs (protein synthesis machinery) along *MTs* or *MFs* (Jansen, 1999) from the nucleus to the strain regions. The translation of mRNAs into proteins then takes place in the sites of the strain. This sequence of events (steps (1) and (2) in Fig. 2(a)) is referred to in our

model as the *synthesis process* of the soluble pool (tetramers).

Since the sources of synthesis are assumed to be associated with the strain regions, their activation is dependent upon the activation of strain. As shown by Chicurel et al. (1998), the ability to cause the ribosome and mRNA relocalization, i.e. the recruitment of the protein synthesis machinery, is correlated with the applied stress as well as with the ability of transmembranar receptors to mediate the mechanical strain. Thus, the intensity of the synthesis in a site is assumed to depend on the strength of the strain acting in this location. Protein synthesis is also assumed to be modulated by the distance separating the intracytoplasmic location from the nucleus. The speed of convergence to the maximum synthesis intensity is inversely proportional to the distance of the nucleus from the sites of synthesis. This hypothesis is used to model the active transport of ribosomes and mRNAs along *MT* or *MF* networks from the nucleus to the strain regions. Moreover, the synthesis process is alternately switched on or off according to specific levels of soluble pool concentration (Fig. 2(b)), which we call the *limiting concentrations*; see (Chou et al., 1993).

The soluble pool spreads through the cytoplasm from the strain regions by *diffusion* (step (3) in Fig. 2(a)) (McGrath et al., 1998). At initial time, we assume that the cell has neither a *CK* filament network nor any soluble *CK*. As *CK* is a cytoplasmic protein (Bray, 1992), the synthesis and the diffusion of the soluble pool are confined to the cytoplasm. As a result, no transmembranar flux takes place.

To summarize, the management of the soluble pool is composed of two processes, the synthesis process and protein diffusion (Fig. 2(b)). Soluble pool concentration fields, resulting from both processes, can be conceived as intracellular strain fields, generated by the intra/extracellular mechanical environment.

2.2. Building up of filaments

Simultaneously to the previously described processes, the building up of filaments begins, starting with *filament nucleation* (Fig. 2(b)). Filaments are initiated at specific sites, called *nucleation centers*. While no site already occupied by a filament can be a nucleation center, an unoccupied site will become one depending on the level of soluble pool concentration in its vicinity. Filament nucleation cannot take place if the concentration is below a critical value (necessary for *ULF* polymerization). Above that value, we associate a degree of nucleation with each site, which we will call the *nucleation susceptibility*. Comparison of the latter with the nucleation properties determines whether a filament can be nucleated at the site. These mechanisms are

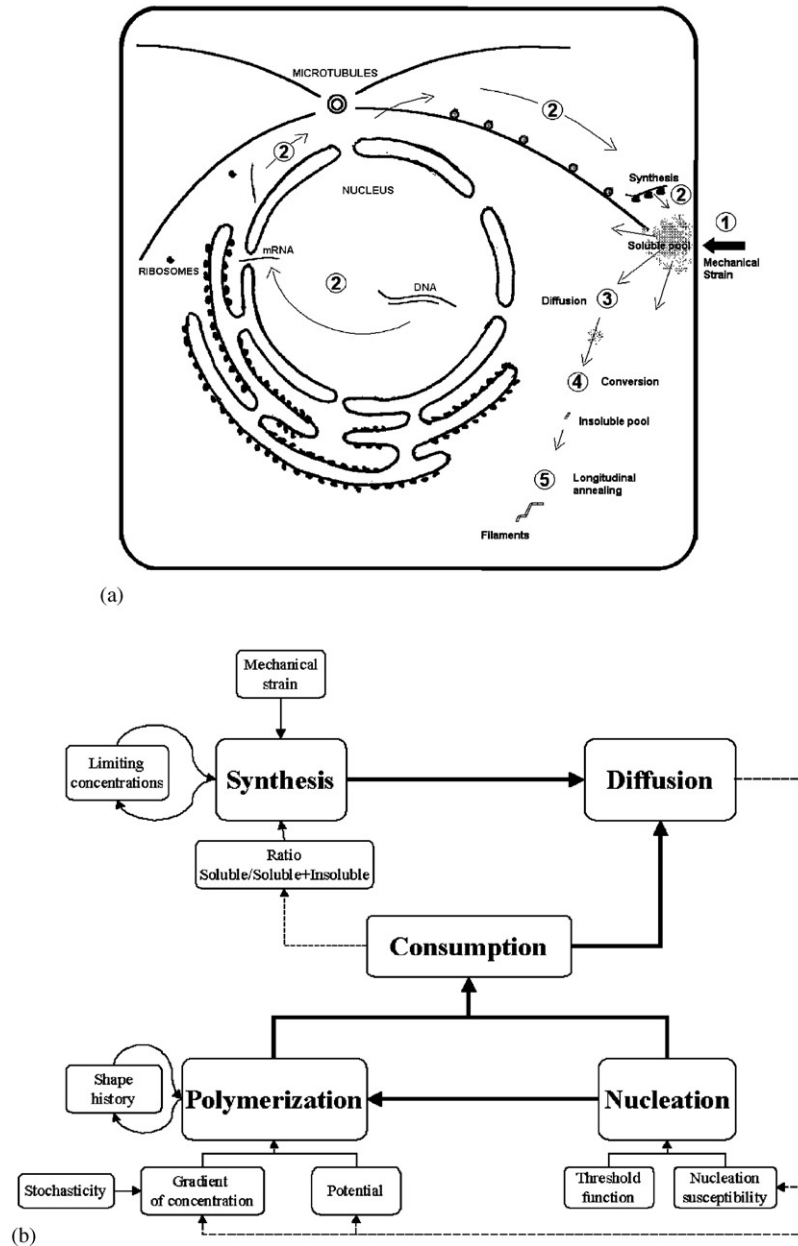


Fig. 2. The model of CK network organization. (a) The action of mechanical strain on the cell (1) induces a protein synthesis (2). The protein synthesis includes several processes, namely transcription, migration of synthesis machinery (messenger RNAs and ribosomes) along MTs (intracellular transport) from the nucleus to the strain regions, and translation into proteins at strain regions. As a result, the protein synthesis produces the soluble pool. The soluble pool spreads through cytoplasm forming concentration fields (3). Then, soluble pool subunits aggregate laterally to form insoluble pool subunits (4). By a longitudinal annealing of insoluble pool subunits to filament tips, filaments grow (5), and the network is built. (b) Extracellular mechanical conditions regulate protein synthesis, which is also modulated by limiting concentrations. Then, as guided by the mechanical environment, the soluble pool propagates by means of a diffusion process. Both synthesis and diffusion are processes related to the soluble pool, whereas the nucleation and the polymerization are related to the insoluble pool. However, the concentration fields of soluble pool partly govern the building up of filaments by taking part in definitions of the nucleation susceptibility, and of both the potential of growth and the environmental contribution. The building up of filaments is jointly directed by the shape history of filaments. Thus, the consumption of soluble pool (or the conversion from soluble to insoluble pool), resulting from the nucleation and the growth of filaments, represents, as a feedback, the response of the filament network to the environment.

represented in the model by functions which are described in Section 3.2.

Next, the building up of the network proceeds by means of longitudinal annealing of ULFs (Herrmann and

Aebi, 2000) from nucleation centers forming filaments (step (5) in Fig. 2(a)). The filament growth is only apical: a filament elongates at its terminal end, the tip of the filament. The filament growth stops when the filament

tip reaches the cell membrane. The creation of the network stems from an anastomosis phenomenon, which is not described in the model, but is expected as an emergent feature of the model.

The longitudinal annealing of *ULFs*, i.e. the filament growth, is governed by both their local interactions with the environment and their non-local interactions via their past history (Fig. 2(b)). The fluctuations of the shape and size of filaments are directed both by the forces applied to the filament as well as by the mechanical properties of the filaments.

As mentioned in Section 2.1, the soluble pool concentration fields represent the strain fields occurring in the cell. The concentration gradient is used to represent the forces to which the tip of the filament is subjected. This environment contribution also includes a stochastic term that can be interpreted as thermal agitation.

The total energy of deformation of a filament is proportional to the integral of the square of the local curvature along the length of filament (Boal, 2002). Taking the square root gives the mean curvature. We call it the *shape history*, meaning that this number gives rough information on how deformed (isotropic) or, on the contrary, how straight (anisotropic), the filament has been up to a given time. A relatively high figure will reflect both a rather contorted filament and enough stored energy for the filament to continue to grow in an undulating pattern. A filament grows in size but does not change its shape; during its growth it must preserve a similarity of form that can vary between anisotropy and isotropy. Thus, the mechanical properties of filaments or their ability to deform are described by the mean curvature.

When a filament is nucleated or an *ULF* is added to the tip of a filament, the proportion of soluble pool necessary for the *ULF* polymerization is consumed at the location of nucleation or growth (step (4) in Fig. 2(a)). The environment modulates the filament formation and, as a feedback, filament growth in turn alters the environment through the soluble pool *consumption*. Thus, the dynamics of the soluble pool, on the one hand, and the building up of *IF* network, on the other hand, are governed by two separate processes which are coupled by the consumption, i.e. the conversion of the soluble pool into the insoluble pool.

The main biological and conceptual mechanisms are summarized respectively in Fig. 2(a) and (b).

3. Mathematical model

The model we propose incorporates the processes we just mentioned. We will now describe it in some detail. As already pointed out, no mathematical derivation is undertaken here: mathematics are used only as an expository medium. The mathematical formulation

essentially paraphrases what has been said in words; however, it is instrumental in the construction of the numerical code and lends itself more readily to discussion and possible improvement.

Prior to stating the equations, we set up the general framework: we look at processes taking place inside an epithelial cell, considered a bounded domain Ω in the physical space. The precise geometry of both the cell and its nucleus are not of interest here, so the cell is represented as a cube and the nucleus inside the cell as another smaller cube with its faces parallel to those of the cell. Elements of the cell are listed in Table 1.

Two state variables are used. $C(X, t)$ is the soluble pool density at a spatial location $X \in \Omega$ at time t , describing the concentration of tetramers. $X_\beta(t)$ is the position at time t of the filament tip initiated at the spatial location $\beta \in \Omega$, some time earlier.

3.1. Extracellular mechanical environment and its effects on the intracellular domain

As mentioned in Section 2.2, mechanical stress induces the relocation of ribosomes and mRNAs to strain regions and their subsequent translation into proteins. This process (steps (1) and (2) in Fig. 2(a)) is described by the *synthesis function* $\mathcal{F}(\cdot)$. This synthesis function is made up of two parts, a space and time-dependent function $\phi(\cdot)$, the *synthesis mode*, and a time-dependent function $\chi(\cdot)$, the *control of synthesis* by limiting concentrations. It is defined by

$$\mathcal{F}(X, t) = \phi(X, t)\chi(t), \quad t \geq 0. \quad (1)$$

The synthesis mode $\phi(\cdot)$ (Fig. 3) is the product of a time-dependent logistic function, with space-dependent parameters, by a set function $\varphi(\cdot)$ discussed below:

$$\phi(X, t) = \begin{cases} \varphi(X) \left(1 - e^{-\frac{(t-T(X))^2}{d(X,N)}} \right) & \text{if } t > T(X) \text{ and } X \in \Theta, \\ 0 & \text{otherwise.} \end{cases} \quad (2)$$

The synthesis is first confined to the cytoplasm Θ . The space-dependent function $T(\cdot)$ states the *activation times*

Table 1
Compartments of the spatial domain Ω

Cell	Ω	Convex set of \mathbb{R}^3
Cell membrane	$\partial\Omega$	Boundary of Ω
Hemidesmosomes	H	Disconnected subset of $\partial\Omega$, $H \subset \partial\Omega$
Desmosomes	D	Disconnected subset of $\partial\Omega$, $D \subset \partial\Omega$
Nucleus	N	Convex open subset of Ω , $N \subset \Omega$
Nuclear envelope	∂N	Boundary of N , $\partial N = \bar{N} \setminus N$
Perinuclear region	P	Subset (usually disconnected) of ∂N , $P \subset \partial N$
Cytoplasm	Θ	Non convex connected subset of Ω , $\Theta = \Omega \setminus N$

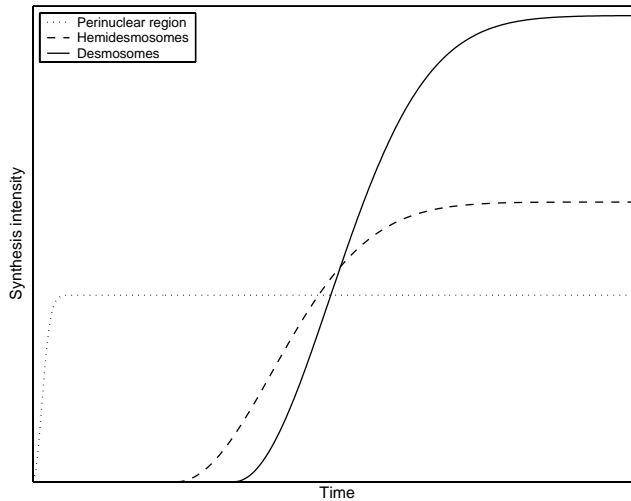


Fig. 3. The modes of protein synthesis, $\phi(\cdot)$, according to the locations in the cell: perinuclear region, hemidesmosomes, and desmosomes. The synthesis, at a given location, differs of the nature of strain applied at this locations. The activation of synthesis depends on the activation time of strain acting at this location. The speed of convergence of the synthesis to the maximal intensity, at a location, is directed by $1/d(\cdot)$ which is the inverse of the distance from this location to the nucleus. The maximal intensity of synthesis at a location is associated with the intensity of strain acting at this location. At all unspecific locations, synthesis is always equal to zero.

of the synthesis sources according to strain activation:

$$T(X) = \begin{cases} t_p, & X \in P, \\ t_h, & X \in H, \\ t_d, & X \in D, \\ \infty, & X \in \Omega \setminus (D \cup H \cup P). \end{cases}$$

t_p represents the activation time of the centripetal field, acting at the perinuclear region to preserve nuclear integrity. The activation time t_h (resp. t_d) corresponds to the time of hemidesmosome (resp. desmosome) establishment. Hence, $0 \approx t_p \ll t_h \ll t_d$. Indeed, we assume, as mentioned in Section 2.2, that the synthesis only begins in the perinuclear region, then is subsequently initiated in the hemidesmosome and desmosome regions.

The slope of the logistic function (2), $1/d(\cdot)$, represents the *speed of convergence* of the synthesis to its maximal intensity, and describes the active transport of protein synthesis machinery along *MTs* or/and *MFs*. The term $d(X, N)$ is the distance from the intracellular location X to the nucleus N (with a correction term to avoid a division by zero). Thus, the smaller the value of $d(\cdot)$ at a location X , the steeper the slope of the logistic function at that point.

Finally, $\varphi(\cdot)$ describes the *intensity of the synthesis sources* in Eq. (2). Despite the fact that cadherins seem to transmit less mechanical stress than integrins (Potard et al., 1997), we assume that the cell–cell connections are stronger than the cell–ECM attachments. Finally, cohesion strain acting around the nucleus is assumed to

be the weakest. The strain magnitudes are not precisely quantified, but according to the above assumed hierarchy and the proportionality to the stress applied (Chicurel et al., 1998), $\varphi(\cdot)$ takes distinct values, φ_d in the desmosomes D , φ_h in the hemidesmosomes H , and φ_p in the perinuclear region P ($\varphi_d > \varphi_h > \varphi_p > 0$). Elsewhere, no synthesis takes place, that is, $\varphi(\cdot) = 0$.

The synthesis function $\mathcal{F}(\cdot)$ is thus modulated by $\phi(\cdot)$, which integrates the location of strain, its activation time, and its intensity (Fig. 3). Moreover, the synthesis is controlled by limiting concentrations, via $\chi(\cdot)$ (Eq. (1)).

The function $\chi(\cdot)$ is defined in terms of the *Heaviside function*,

$$\mathcal{H}(x) = \begin{cases} 0, & x < 0, \\ 1, & x \geq 0. \end{cases} \quad (3)$$

by

$$\chi(t) = \mathcal{H}(\bar{C} - Q(t))[\mathcal{H}(\pi\bar{C} - Q(t)) + \mathcal{H}\left(\frac{1}{1-\eta}\Gamma(t) - Q(t)\right)\mathcal{H}(Q(t) - \pi\bar{C})], \quad (4)$$

where $Q(t)$ describes the total quantity of *CK* produced up to time t in the cell, i.e. the state of both the *soluble and insoluble pools* at time t

$$Q(t) = \int_0^t \int_{\Omega} \phi(u, \tau) du d\tau. \quad (5)$$

The term $\Gamma(t)$ in Eq. (4) represents the total consumption of the soluble pool due to the assembly of tetramers into *ULF* through nucleation and growth over the time interval from the initial time to time t . $\Gamma(t)$ can also be considered as the total quantity of the *insoluble pool* at time t in the cell domain,

$$\Gamma(t) = \int_0^t \sigma_{min} \int_{\Omega} \mathbb{1}_{\rho(s) \cup \mathcal{B}(s)}(t) dt ds, \quad (6)$$

where σ_{min} represents the *critical concentration* of soluble pool necessary for *ULF* constitution. $\rho(t)$ is the set of filament tips which are actually growing at time t , and $\mathcal{B}(t)$ is the set of sites where a filament is nucleated at time t .

At time t , synthesis is allowed as long as the quantity $Q(t)$ of *CK* synthesized up to this time (see Eq. (5)) is less than the limit concentration \bar{C} (soluble and insoluble pools): this control is modeled by the first term of the right-hand side of Eq. (4), $\mathcal{H}(\bar{C} - Q(t))$. It is also assumed that synthesis will continue freely until $Q(t)$ reaches a fraction π of the maximal concentration \bar{C} above which it stops. This hypothesis is described by the term $\mathcal{H}(\pi\bar{C} - Q(t))$ in Eq. (4). According to the literature (Chou et al., 1993), the soluble pool has to account for at least a fraction η of the total *CK* in the cell ($\eta = \text{total } \mu\text{g of soluble CK} / \text{total } \mu\text{g of CK in cell}$), which is expressed by $(Q(t) - \Gamma(t))/Q(t) \geq \eta$. This control by the ratio of soluble pool to total *CK*, represented by $\mathcal{H}([1/(1-\eta)]\Gamma(t) - Q(t))$, is only

activated after the initiation of the synthesis process. This delayed control is accounted for by the multiplication by the term $\mathcal{H}(Q(t) - \pi\bar{C})$.

The synthesis function $\mathcal{F}(\cdot)$ defined by Eq. (1), controlled and modulated by $\chi(\cdot)$ and $\phi(\cdot)$ respectively, generates the soluble pool which, from its sites of production, *diffuses* throughout the cytoplasm. We assume a constant diffusion rate D , so that the equation governing the dynamics of the soluble pool reads as

$$\frac{\partial C}{\partial t} = D(\Delta_x C) + \mathcal{F} = D\left(\frac{\partial^2 C}{\partial x^2} + \frac{\partial^2 C}{\partial y^2} + \frac{\partial^2 C}{\partial z^2}\right) + \mathcal{F}. \quad (7)$$

For simplicity, it is assumed that at time $t = 0$, no CK is present in the cell, that is,

$$\forall X \in \Omega, \quad C(X, 0) = 0. \quad (8)$$

The diffusion equation also proceeds under zero flux boundary conditions at the boundary $\partial\Theta$ of the cytoplasm, which is defined as the union of the cellular membrane $\partial\Omega$ and the nuclear envelope ∂N .

$$\frac{\partial C}{\partial n}|_{\partial\Theta} = 0 \Leftrightarrow \begin{cases} \frac{\partial C}{\partial n}|_{\partial\Omega} = 0, \\ \frac{\partial C}{\partial n}|_{\partial N} = 0. \end{cases} \quad (9)$$

The PDE (7), with conditions (8) and (9), generates scalar fields of soluble pool concentration, which represent intracellular force fields generated by the mechanical environment. The CK network is built up from these fields of soluble pool concentration.

3.2. Building up of filaments

As mentioned in Section 2.2, the starting point for a filament is *nucleation* which occurs at specific intracellular locations, called nucleation centers. Such centers are recruited amongst unoccupied sites as follows; we first define the *nucleation susceptibility* $\lambda(\beta, t)$ of a site β at time t ,

$$\lambda(\beta, t) = \begin{cases} 0 & \text{if } C(\beta, t) \leq \sigma_{min}, \\ \mathbb{1}_{\Omega \setminus \mathcal{S}(t)}(\beta) [1 - e^{-a(C(\beta, t) - \sigma_{min})^2}] & \text{if } C(\beta, t) > \sigma_{min}, \end{cases} \quad (10)$$

where a is a positive constant. The logistic function is used to model the property of tetramers to spontaneously aggregate instantly forming *ULF*, when the soluble pool concentration increases up to a critical concentration σ_{min} . Below σ_{min} , neither nucleation nor longitudinal annealing can take place (Fig. 4).

The characteristic function $\mathbb{1}_{\Omega \setminus \mathcal{S}(t)}(\cdot)$ tests whether a given site belongs to $\mathcal{S}(t)$. The set $\mathcal{S}(t)$ denotes the region filled by the filaments at time t , $\mathcal{S}(t) = \bigcup \{X_\beta(s) : \beta \in \mathcal{B}(\sigma), \sigma \leq s \leq t\}$. Thus, if a location β

belongs to $\mathcal{S}(t)$, that is, if β belongs to a filament, then no additional filament will be nucleated at β .

The *recruitment function* $\mathcal{R}(\cdot)$ is defined $\forall \beta \in \Omega$ by

$$\mathcal{R}(\beta)(t) = \mathcal{H}(\lambda(\beta, t) - p(\beta)) = \begin{cases} 0 & \text{no nucleation (i.e. } \lambda(\beta, t) < p(\beta)), \\ 1 & \text{nucleation (i.e. } \lambda(\beta, t) \geq p(\beta)). \end{cases} \quad (11)$$

$\mathcal{R}(\cdot)$ compares the nucleation susceptibility $\lambda(\beta, t)$ at a site β at time t to a threshold function $p(\beta)$. This function $p(\cdot) \in (0, 1]$ can be either a constant or a space-dependent function which describes *privileged regions for nucleation*. In the case of a space-dependent function, $p(\cdot)$ can be defined as a function directly or inversely proportional to the distance separating an intracytoplasmic location from the nucleus (Fig. 4). Thus, the nucleation can be respectively restricted around the nucleus or in the cell cortex.

So, at time t , β is a nucleation center if the recruitment function $\mathcal{R}(\beta)(t)$ is equal to 1, that is to say, $\mathcal{B}(t) = \{\beta : \mathcal{R}(\beta)(t) = 1\}$. It is also useful to define the set $\mathcal{I}(t)$ of nucleation centers β initiated *before* time t , namely $\mathcal{I}(t) = \{\beta : \mathcal{R}(\beta)(s) = 1, \text{ for some } s, s < t\} = \bigcup_{0 \leq s < t} \mathcal{B}(s)$.

Now $X_\beta(\cdot)$ is a parametric curve in the physical space whose image represents the filament nucleated at β , at some time $d_i(\beta) = t_0$; $X_\beta(t)$ is the position at time t of the tip of the filament nucleated at β . We also define $d_b(\cdot) = t_\infty$ as the time when the filament reaches the cell membrane. It can also be defined as $d_b(\beta) = \inf_t \{t > d_i(\beta) : X_\beta(t) \in \partial\Omega\}$.

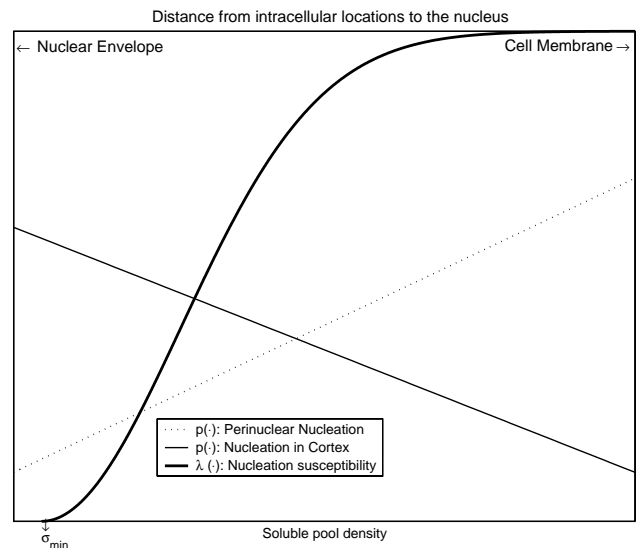


Fig. 4. The nucleation susceptibility $\lambda(\cdot)$ (for a location unoccupied by filaments), and two space-dependent threshold functions $p(\cdot)$. $\lambda(\cdot)$ is function of soluble pool concentration. If the soluble pool concentration at the site is lower than σ_{min} , then its nucleation susceptibility is equal to zero. $p(\cdot)$ allows to specify the preferential regions for nucleation. At each location, $p(\cdot)$ defines a threshold for $\lambda(\cdot)$. The function $p(\cdot)$, denoted “Perinuclear nucleation”, favors the nucleation around the nucleus. On the other hand, using $p(\cdot)$ labelled “Nucleation in Cortex”, favors the nucleation in the cell cortex.

Finally, it is useful to define the set $\mathcal{I}_b(t)$ of initial conditions of solutions $X_\beta(\cdot)$ nucleated before time t and having reached the boundary at time t or some time earlier, $\mathcal{I}_b(t) = \{\beta \in \mathcal{I}(t) : X_\beta(s) \in \partial\Omega, \text{ for some } s, s \leq t\}$. Then, when a filament tip reaches the boundary $\partial\Omega$, the solution $X_\beta(\cdot)$ adopts a stationary behavior $X_\beta(t) = X_\beta(t_\infty), t_\infty \leq t$. Hence,

$$\forall \beta \in \mathcal{I}_b(t), \quad \frac{dX_\beta(t)}{dt} = 0. \tag{12}$$

The *dynamics of filaments* depend on whether the filament tip has reached the boundary $\partial\Omega$ of the domain. If the tip is still in the domain, i.e. $\forall \beta \in \mathcal{I}(t) \setminus \mathcal{I}_b(t)$, the filament grows by an *apical longitudinal annealing of ULF* from its nucleation center and later from its filament tips.

Let us now describe the function defining the growth rate of a filament. We consider a filament nucleated at site β . We give below an expression of the growth rate at a time t , when the tip of the filament has not reached the boundary of the cell, that is, such that β belongs to $\mathcal{I}(t) \setminus \mathcal{I}_b(t)$. In order for the filament to grow, it is necessary that the soluble pool concentration in the vicinity of the filament tip be above a critical value σ_{min} , a threshold for the aggregation of tetramers into *ULF*. We define the function

$$\mathcal{E}(X, t) = \begin{cases} 0 & \text{if } \int_{N_X} (C(y, t) - \sigma_{min}) dy < 0, \\ 1 & \text{if } \int_{N_X} (C(y, t) - \sigma_{min}) dy \geq 0, \end{cases} \tag{13}$$

which evaluates the *local state of the soluble pool* in a neighborhood N_X of the point X . $\mathcal{E}(X, t) = 0$ means

(i.e. the local magnitude and the direction of the mechanical strain field). Here, v is a three-dimensional random vector which follows a uniform law on $[-u, u]^3$ with $u \in \mathbb{R}^+$ small enough. Indeed, this stochastic term should not become the predominant component of the environment contribution. ε is a small positive parameter intended to correct for possible spurious behavior due to the vanishing of the denominator (hence, $0 < \varepsilon \ll 1$).

The filament grows in size but does not remodel its shape during its growth, it must preserve a similarity of form. The filament contribution to the longitudinal annealing is based on *mechanical properties of the filaments*. It is described by the quantity

$$\frac{\int_{d_i(\beta)}^t |\kappa(X_\beta(u))| du}{t - d_i(\beta)} \frac{X'_\beta(t_-)}{\|X'_\beta(t_-)\| + \varepsilon}.$$

The vector $X'_\beta(t_-)/(\|X'_\beta(t_-)\| + \varepsilon)$ points in the direction of the vector tangent to the solution $X_\beta(\cdot)$ at point $X_\beta(t)$, the tip of filament at time $t_- = t - \delta$, for some $\delta, 0 < \delta \ll 1$. It represents the velocity of filament $X_\beta(\cdot)$ at time t taking into account the past through the left-hand derivative. The function $\kappa(X_\beta(t))$, defined in Eq. (A.4) (Section A.3), represents the curvature of the filament nucleated at β at the point $X_\beta(t)$. The term $\int_{d_i(\beta)}^t |\kappa(X_\beta(u))| du / (t - d_i(\beta))$ is the *mean curvature*; it is the value we retain as an indicator of the shape of the filament or the *shape history* of the filament.

Thus, the filament growth by apical longitudinal annealing of *ULF* is governed by the following system of SDEs:

$$\frac{dX_\beta(t)}{dt} = \begin{cases} \mathcal{E}(X_\beta(t), t) \left[\frac{(\nabla_X C)(X_\beta(t), t) + \|(\nabla_X C)(X_\beta(t), t)\|v}{\|(\nabla_X C)(X_\beta(t), t)\| + \varepsilon} + \frac{\int_{d_i(\beta)}^t |\kappa(X_\beta(u))| du}{t - d_i(\beta)} \frac{X'_\beta(t_-)}{\|X'_\beta(t_-)\| + \varepsilon} \right] & \forall \beta \in \mathcal{I}(t) \setminus \mathcal{I}_b(t), \\ 0 & \forall \beta \in \mathcal{I}_b(t) \end{cases}$$

that no growth is possible, while $\mathcal{E}(X, t) = 1$ indicates that longitudinal annealing can be carried out. Growth is then controlled both by local interactions with the environment (the *environment contribution*) and non-local interactions (the *filament contribution*).

The environment contribution describes the *net force applied to the filament tip* (mechanical strain and thermal agitation) in terms of soluble pool density fields and stochastic term. The strain field is represented by the vector function

$$\frac{(\nabla_X C)(X, t) + \|(\nabla_X C)(X, t)\|v}{\|(\nabla_X C)(X, t)\| + \varepsilon},$$

which combines the *local concentration gradient* $(\nabla_X C)(X, t)$ and a *stochastic term* v . The steepness of the local gradient depends on the rate of flux and the direction of flow in the soluble pool concentration field

with the initial conditions $X_\beta(d_i(\beta)) = \beta$. The set $\rho(t)$ of the tips which are actually growing at time t , is defined by $\rho(t) = \{X_\beta(t) : \beta \in \mathcal{I}(t) \setminus \mathcal{I}_b(t), dX_\beta/dt_i \neq 0\}$.

3.3. Coupling of the environment and the filament building up

During both filament nucleation and longitudinal annealing, the *soluble pool is consumed and converted into insoluble pool*. The total consumption $\Gamma(t)$, from the initial time to time t , is defined by Eq. (6) and the soluble pool consumption rate, at time t , is governed by

$$\frac{d}{dt} \Gamma(t) = \sigma_{min} \int_{\Omega} \mathbb{1}_{\rho(t) \cup \mathcal{B}(t)}(t) dI,$$

which expresses the instant global rate of consumption as the integral of the local consumption rate at both the nucleation centers and the tips of filaments. Thus the conversion of the soluble into the insoluble pool couples, in effect, the environment (where the tetramers are produced and transported) and the filaments where they fix themselves.

3.4. Governing equations

The above considerations lead to the following system of PDE and SDE equations:

$$\frac{\partial C(X, t)}{\partial t} = \underbrace{D(\Delta_X C)(X, t)}_{\text{diffusion}} + \underbrace{\mathcal{F}(X, t)}_{\text{synthesis}} - \underbrace{\left(\underbrace{\sigma_{\min} \mathbb{1}_{\mathcal{B}(t)}(X)}_{\text{nucleation}} + \underbrace{\sigma_{\min} \mathbb{1}_{\rho(t)}(X)}_{\text{annealing}} \right)}_{\text{consumption}}, \quad (14)$$

$$\frac{dX_\beta}{dt} = \begin{cases} \underbrace{\mathcal{E}(X_\beta(t), t)}_{\text{potential}} \underbrace{\left[\frac{(\nabla_X C)(X_\beta(t), t) + \|(\nabla_X C)(X_\beta(t), t)\|v}{\|(\nabla_X C)(X_\beta(t), t)\| + \varepsilon} \right]}_{\text{environment control}} \\ + \underbrace{\left[\frac{\int_{d_i(\beta)}^t |\kappa(X_\beta(u))| du}{t - d_i(\beta)} \frac{X'_\beta(t_-)}{\|X'_\beta(t_-)\| + \varepsilon} \right]}_{\text{filament control}} \\ 0 \end{cases} \quad (15)$$

$$\forall \beta \in \mathcal{I}(t) \setminus \mathcal{I}_b(t),$$

$$\forall \beta \in \mathcal{I}_b(t)$$

with initial conditions $\forall X \in \Omega, C(X, 0) = 0$, and $X_\beta(d_i(\beta)) = \beta$ and boundary conditions $\frac{\partial C}{\partial n}|_{\partial \Omega} = 0$. The sets $\mathcal{B}(t), \rho(t)$ and the function $d_i(\beta)$ are defined in Section 3.2.

The first equation (14) governs the dynamics of the soluble pool. It is derived from our phenomenological description of the mechanical environment. It is the sum of three terms, corresponding to diffusion of the soluble pool within the cytoplasm, its synthesis, and its consumption. The consumption term is, in turn, the sum of $\sigma_{\min} \mathbb{1}_{\mathcal{B}(t)}(X)$, which describes the consumption at nucleation centers and $\sigma_{\min} \mathbb{1}_{\rho(t)}(X)$, which describes filament growth.

Eq. (15) describes the growth of filaments and the variations of their geometry. Growth is on or off depending upon the local state as determined by the function \mathcal{E} (13). The term inside the brackets is the sum of two vectors, which gives the direction of growth. The first vector points mainly in the direction of concentration gradient, that is to say, wherever there is fuel for growth. This direction is altered by a random vector whose intensity is small compared to concentration

gradient. The second vector points in the direction tangent to the filament, with intensity proportional to the mean curvature.

Eq. (14) generates scalar fields of soluble pool concentrations, on which the building up of filaments is partly based. In its turn, the consumption of soluble pool, resulting from the formation of filaments, modifies the scalar fields.

The notations used in the model are listed in Tables 1–3.

4. Numerical experiments

From the mathematical model presented in Section 3, a 3D simulation model, outlined in Appendix A, was derived and implemented in the C programming language. The numerical experiments presented below were obtained from simulation runs on a cubic grid formed of 60 mesh points per face (Fig. 12) and using the parameter values given in Table 3.

Two types of outputs are extracted from the simulations: the first depicts the soluble pool concentration fields in the intracellular domain resulting from the mechanical strain (Fig. 5), the other represents the CK network (Figs. 6–8). First, the soluble pool concentration fields are visualized by volumetric representations. The soluble pool densities are represented on a scale of gray, where the darkest gray (black) corresponds to the lowest density and the lightest gray (white) corresponds to the highest density (Fig. 5). Secondly, the CK network is visualized as images generated with the PovRay Ray-Tracer (Figs. 6–8).

After 15 min, only a centripetal force field preserving the nuclear integrity acts around the nucleus (Fig. 5(a)). At this instant, a unique source confined to the perinuclear region provides proteins that spread through the cytoplasm. At $t = 30$ min (Fig. 5(a)), hemidesmosomes and desmosomes have formed. The lighter gray patches on the lateral surfaces (resp. on the basal surface) match the desmosome regions (resp. hemidesmosome regions). These regions correspond to new

Table 2
Sets and functions used in the model

$C(X, t)$	Soluble pool density at point X at time t
$X_\beta(\cdot)$	Filament nucleated at β
$X_\beta(t)$	Tip, at time t , of the filament nucleated at β
$\mathcal{F}(X, t)$	Protein synthesis function at point X at time t
$\phi(X, t)$	Mode of protein synthesis at point X at time t
$\varphi(X)$	Intensity of the protein synthesis at point X
$T(X)$	Activation time of strain at point X
$d(X, N)$	Distance from point X to the nucleus N
$\chi(t)$	Control of protein synthesis at time t
$Q(t)$	Total quantity of CK produced at time t
$\Gamma(t)$	Total consumption of soluble pool from the initial time to time t
$\lambda(X, t)$	Susceptibility of nucleation at point X at time t
$\mathcal{S}(t)$	Union of all filaments at time t
$p(\cdot)$	Threshold function
$\mathcal{R}(X)(t)$	Recruitment function to nucleate filament at point X at time t
$\mathcal{B}(t)$	Set of initial conditions of solutions initiated at time t
$d_i(\beta)$	Initiating time of the filament of initial condition β
$d_b(\beta)$	Terminating time of the filament of initial condition β
$\mathcal{E}(X, t)$	Potential of growth at point X and time t
$\kappa(X)$	Curvature of filament at point X
$\mathcal{I}(t)$	Set of initial conditions of solutions initiated before time t
$\mathcal{J}_b(t)$	Set of initial conditions of solutions initiated before time t and having reached the domain boundary at some time before t
$\rho(t)$	Set of new tips which actually grow at time t
v	Stochastic term

protein synthesis regions. After 1 h, the synthesis continues and the soluble pool keeps on spreading through the cytoplasm (Fig. 5(c)). After 2 h, the synthesis has stopped, and only residual consumption and diffusion occur (Fig. 5(d)). Over the next few hours ($t = 5$ and 25 h), the soluble pool propagates and tends to homogenize the concentrations (Fig. 5(e) and (f)).

Depending on the chosen regions for nucleation, the filaments are initiated in the cell cortex (Fig. 6), in the perinuclear region (Fig. 7) or anywhere in the cytoplasm (Fig. 8).

For nucleation in the cortex using the same parameters as in Fig. 5, filaments are initiated in the desmosome plaques (Fig. 6(a)), loci where the synthesis intensity is the largest. This occurs after 40 min, i.e. 20 min after desmosome establishment. After 8 min, more filaments are also nucleated on the basal surface at the hemidesmosome plaques (Fig. 6(b)). Before spreading through the cell, filaments first carpet the desmosome plaques until $t = 56$ min (Fig. 6(b) and (c)). Progressively, filaments reach the perinuclear region and establish a link from the cell membrane to the nucleus envelope (Fig. 6(c)–(f)). At $t = 104$ min, the CK network is stable (Fig. 6(f)).

For perinuclear nucleation with a diffusion coefficient twice as big as that of Fig. 6, filaments start at $t = 4$ min (Fig. 7(a)) and grow from the perinuclear region, forming a cage which surrounds the nucleus (Fig. 7(a)–

Table 3
Parameters used in the model

l	Length of cell domain Ω	20 μm
D	Diffusion coefficient of soluble pool through the cytoplasm	$[5 \times 10^{-4}, 10^{-2} \mu\text{m}^2\text{s}^{-1}]^a$
σ_{min}	Critical soluble pool concentration	1–10 μM^b
\bar{C}	Maximal CK concentration for a cell	0.5–0.9%
η	Ratio of soluble pool to total CK	5% ^c
π	Fraction of maximal concentration \bar{C} to prime the dynamics	20–50% ^d
t_p	Activation time of centripetal field acting at the perinuclear region	0 min ^d
t_h	Activation time of force acting at hemidesmosome areas	15 min ^b
t_d	Activation time of force acting at desmosome areas	20 min ^b
φ_p	Intensity of protein synthesis at a site belonging to perinuclear region	$\simeq 30 \text{ nM}^b$
φ_h	Intensity of protein synthesis at a site belonging to hemidesmosome regions	$\simeq 40 \text{ nM}^b$
φ_d	Intensity of protein synthesis at a site belonging to desmosome regions	$\simeq 60 \text{ nM}^b$
$p(\cdot)$	Threshold function	^d
$\ v\ $	Magnitude of stochastic term	$5 \times 10^{-3} - 0.25^d$

^aSee Section 4.1.

^bTo the best of our knowledge there are no estimates of such values in the literature. We chose the proposed values to obtain realistic results on the stabilization time.

^cChou et al. (1993).

^dModeling hypothesis.

(c)). After 25 min, filaments spread through the cell membrane, at first in the direction of the basal surface (Fig. 7(d)) and, after a while, in the direction of the lateral surfaces (Fig. 7(c)). Thus, a network connecting the nuclear envelope to the cell membrane is built and stabilizes after only 36 min (Fig. 7(f)).

If we take $p(\cdot)$ to be a constant function, assuming that nucleation takes place at an equal rate everywhere, with the same parameters as in Fig. 7, then the first filaments are initiated at $t = 22$ min from the desmosome plaques (the regions where the synthesis intensity is largest). The nucleation process then reaches the hemidesmosome plaques (Fig. 8(a) and (b)) and extends finally to the perinuclear region (the region where the synthesis intensity is smallest) 5 min later (Fig. 8(c)). As in the previous two cases, propagation from the cortex and from the perinuclear region is preceded for 30 min by filament carpeting of the desmosome and hemidesmosome plaques, and by filament surrounding of the nucleus (Fig. 8(d)). At $t = 42$ min, the CK network reaches a steady state (Fig. 8(f)).

Thus, whatever the privileged region for nucleation, filaments grow through the cell, forming a network

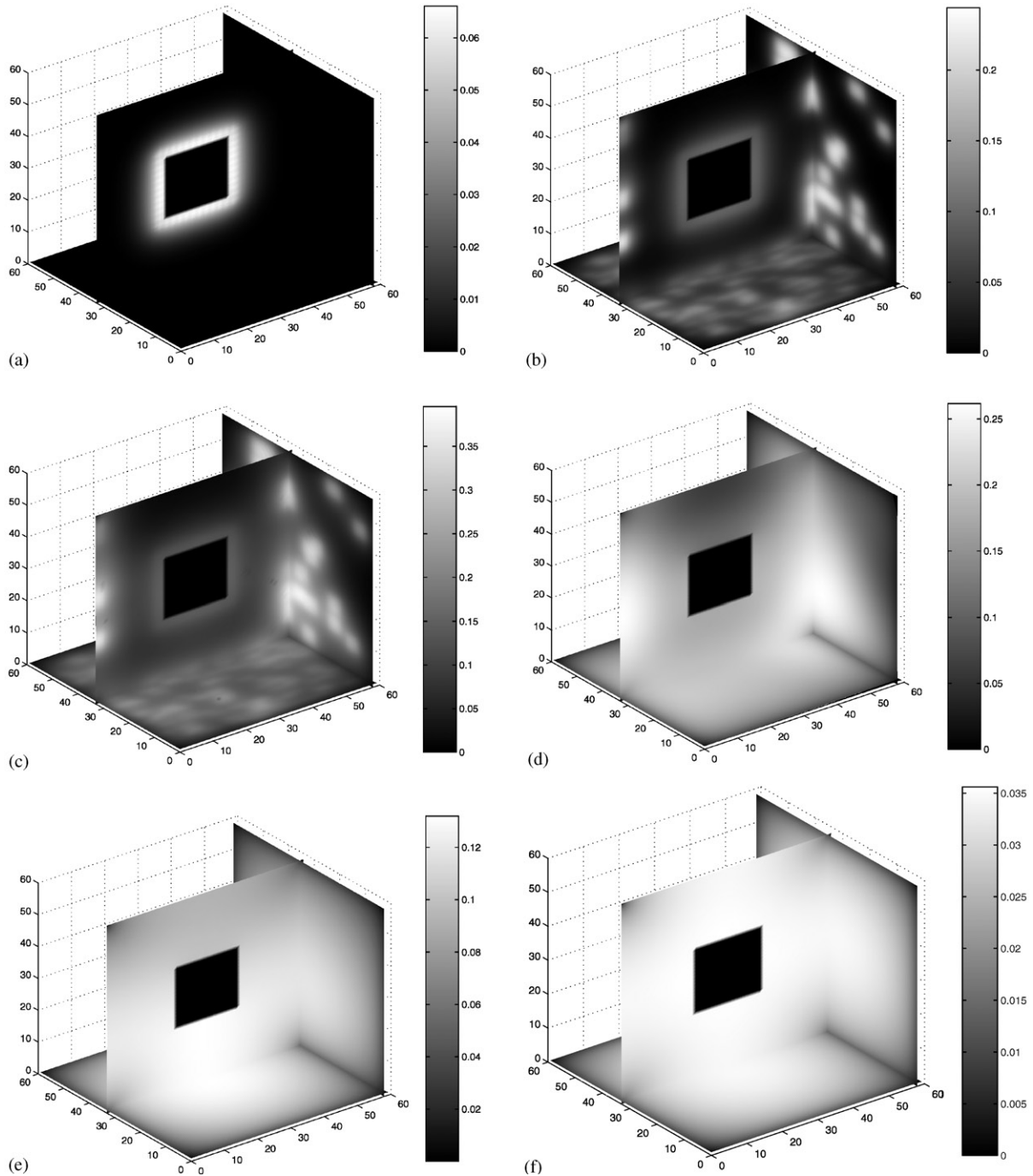


Fig. 5. Evolution of concentration fields of soluble pool ($D = 5 \times 10^{-3} \mu\text{m}^2 \text{s}^{-1}$). From the cell volumetric representation only three planes are represented: an horizontal plane representing the basal surface of the epithelial cell, a first vertical plane crossing the nucleus that is the interior black square and a second vertical plane corresponding to the lateral face of the cell where are located desmosome plaques. The soluble pool concentrations are represented by the gray scale that is depicted in colorbars.

which links the cell membrane to the nuclear envelope (Figs. 6(f)–8(f)). Eventually, the network tends to stabilize.

Depending on the parameter values of the model, the CK network adopts different architectures formed by filaments having specific characteristics. To quantify the architecture of networks, we have extracted some

features characterizing the network in terms of density (the total number of filaments) and the filament morphology (the mean filament length and the mean filament curvature). The length of a filament $X_\beta(\cdot)$ is defined as its arclength, that is to say, $\int_{d_i(\beta)}^{d_b(\beta)} \sqrt{x'_\beta(t)^2 + y'_\beta(t)^2 + z'_\beta(t)^2} dt$. In terms of these

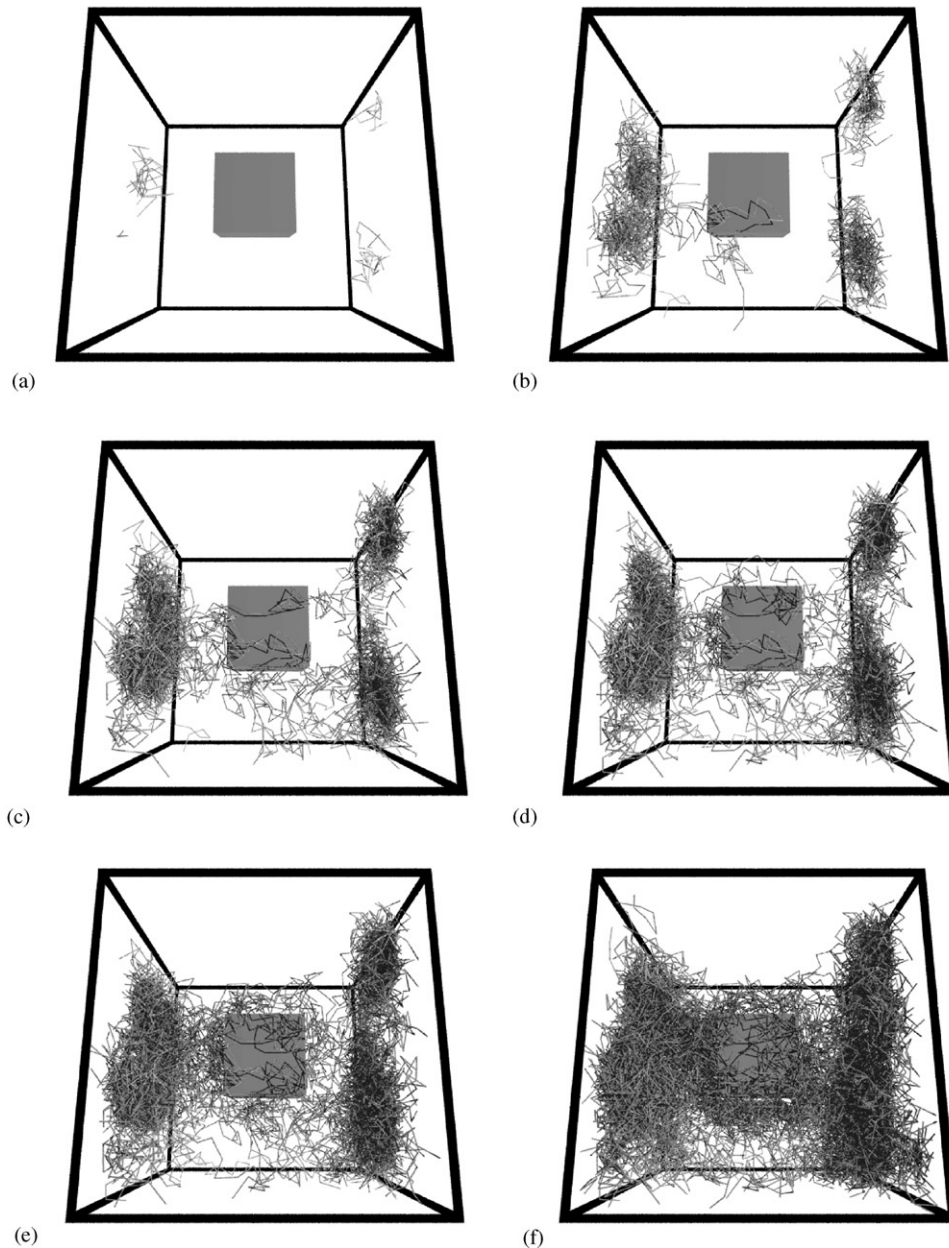


Fig. 6. The CK network at several times, for the parameters of Fig. 5 and a nucleation in the cell cortex. (a) At 40 min, few filaments are nucleated in the cell cortex from the desmosome plaques, where the synthesis intensity is the highest. (b–f) A network, linking the cell membrane to the perinuclear region, is established. (f) At 104 min, the CK network is stabilized.

features, we have studied the influence of different parameters, namely, we focused on three: the diffusion coefficient, the nucleation regions and the stochastic term.

4.1. Influence of the diffusion coefficient

As far as we know, an accurate value of the diffusion coefficient for CK proteins is not known. The diffusion coefficient D of a particle in a solution can be estimated from the well-known Stokes–Einstein law defined as the ratio of the thermal energy ($k_B T$, where k_B is the Boltzmann constant and T is the temperature in Kelvin)

to the drag coefficient. The latter depends on the viscosity of the solution, on the shape of the particle, and on the orientation with respect to the direction of the flow. To estimate D for CK tetramers we first evaluate the drag coefficient for a spherical particle with the actin monomer dimensions (4 nm of diameter). With the CK tetramer dimensions (3 nm of diameter and 50 nm of length), we also estimate the drag coefficient for a cylindrical particle (Howard, 2001). This allows us to estimate orders of magnitude between the two types of objects. For actin, the diffusion coefficient is known in some experimental settings (McGrath et al., 1998).

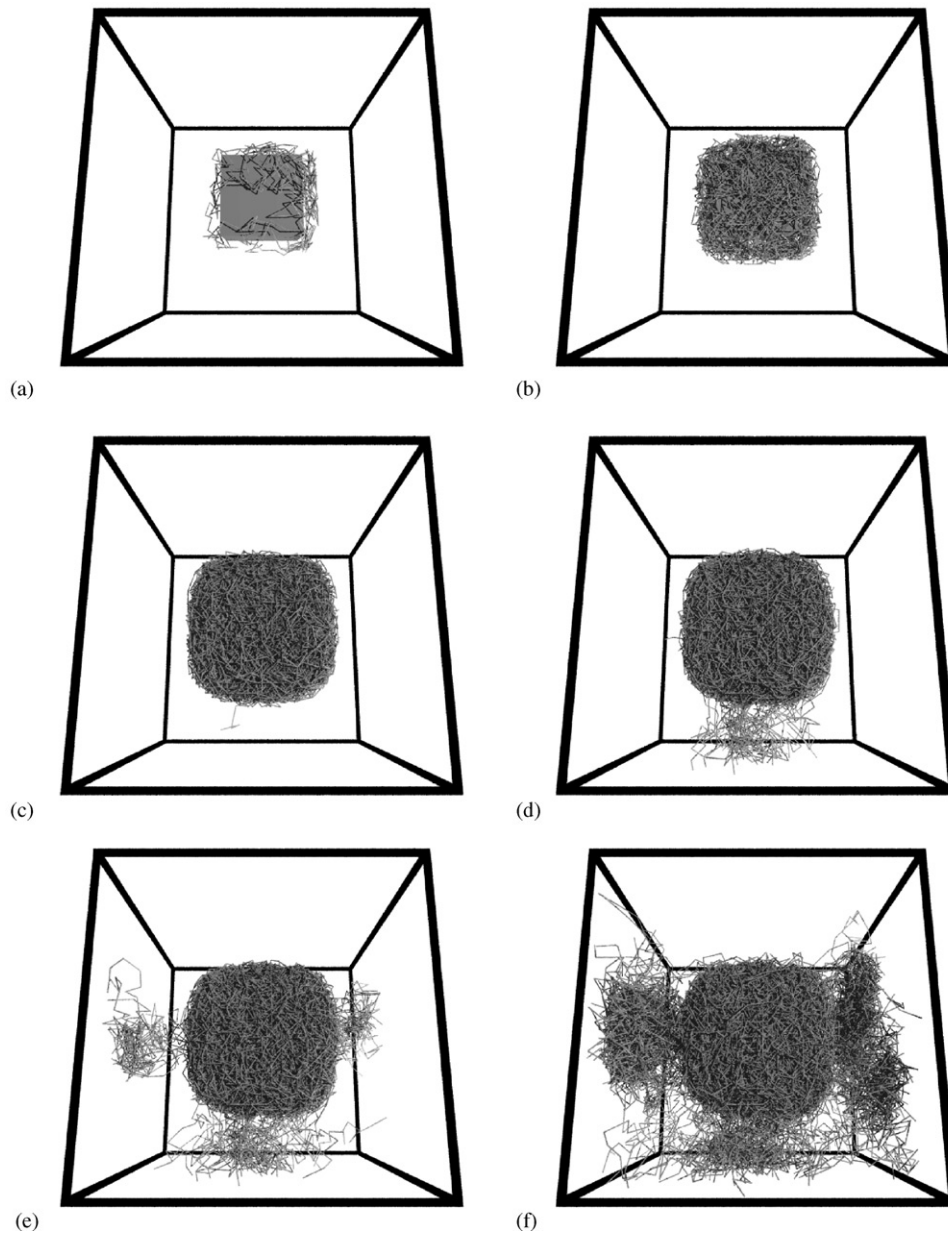


Fig. 7. The CK network at several times for a diffusion coefficient $D = 10^{-2} \mu\text{m}^2 \text{s}^{-1}$ with a perinuclear nucleation. (a) At 4 min, few filaments are nucleated in the perinuclear region. (b–c) A network builds up in the perinuclear region, forming a cage around the nucleus. (d–f) A network, linking the perinuclear region to the cell membrane, is established. (f) At 36 min, the CK network is stabilized.

From this, we deduce estimated values of D for a CK tetramer on the order of $10^{-2} \mu\text{m}^2 \text{s}^{-1}$. We use diffusion coefficients for CK tetramers ranging from 5×10^{-4} to $10^{-2} \mu\text{m}^2 \text{s}^{-1}$. The lower figure is an estimate that combines the information provided by estimation and a hypothesis of a weaker diffusion.

The slower the diffusion process, the more the soluble pool accumulates near synthesis regions. Since nucleation depends on a critical concentration, this accumulation induces an earlier onset of nucleation. For a diffusion coefficient $D = 5 \times 10^{-4} \mu\text{m}^2 \text{s}^{-1}$, nucleation starts 6 min after the beginning of the simulation,

whereas for a diffusion of $D = 10^{-2} \mu\text{m}^2 \text{s}^{-1}$, it takes 30 min to start (Fig. 9a). Moreover, this accumulation mechanism also plays a role in the network density. Indeed, the total number of filaments also depends on the diffusion. The faster the diffusion process, the less numerous the filaments are at the end. For a diffusion coefficient of $D = 10^{-2} \mu\text{m}^2 \text{s}^{-1}$, the number of filaments rises to 2535, whereas for $D = 5 \times 10^{-4} \mu\text{m}^2 \text{s}^{-1}$, the number of filaments is 11 060 at stabilization (Fig. 9(a)). In contrast to its influence on the number of filaments, the mean filament length is not very sensitive to the diffusion coefficient. The mean filament

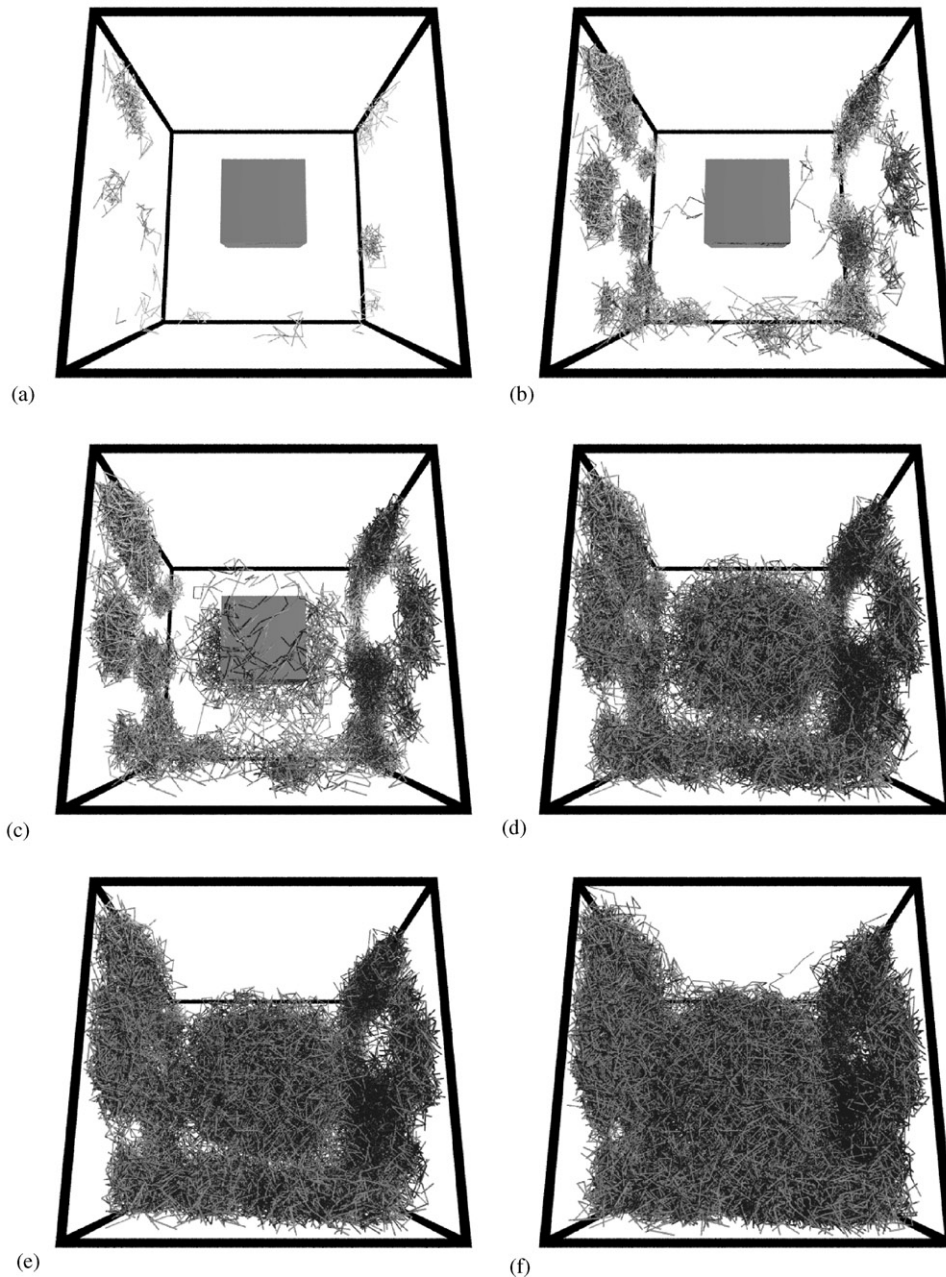


Fig. 8. The CK network at several times for the same parameters of Fig. 7, but with no preferential regions for nucleation ($p(\cdot) = 0.2$). (a) At 22 min, filaments are nucleated in the cell cortex from the desmosome plaques. (b–f) A network, linking the cell membrane to the perinuclear region, is established. (f) At 42 min, the CK network is stabilized.

length varies from 14.20 ± 20.85 , for $D = 10^{-2} \mu\text{m}^2 \text{s}^{-1}$, to 19.49 ± 96.82 , for $D = 10^{-3} \mu\text{m}^2 \text{s}^{-1}$ (Fig. 9(b)). On the other hand, the mean filament curvature seems to show a correlation with diffusion (Fig. 9(c)). The lower the diffusion process, the more filaments adopt a rectilinear behavior. The value $D^* = 10^{-3} \mu\text{m}^2 \text{s}^{-1}$ divides the set of values of the diffusion into two regions. For $D < D^*$, the model adopts roughly the same behavior: with similar times to stabilization and similar values when the system is stabilized. These behavioral

differences separated according to a threshold value D^* could be interpreted as a change in the relevance of the value of the diffusion coefficient.

4.2. Influence of the nucleation regions via $p(\cdot)$

The nucleation regions seem to influence neither the mean filament length nor the mean filament curvature, even if a perinuclear nucleation produces filaments which tend to be longer and wavier (Fig. 10(b) and (c)).

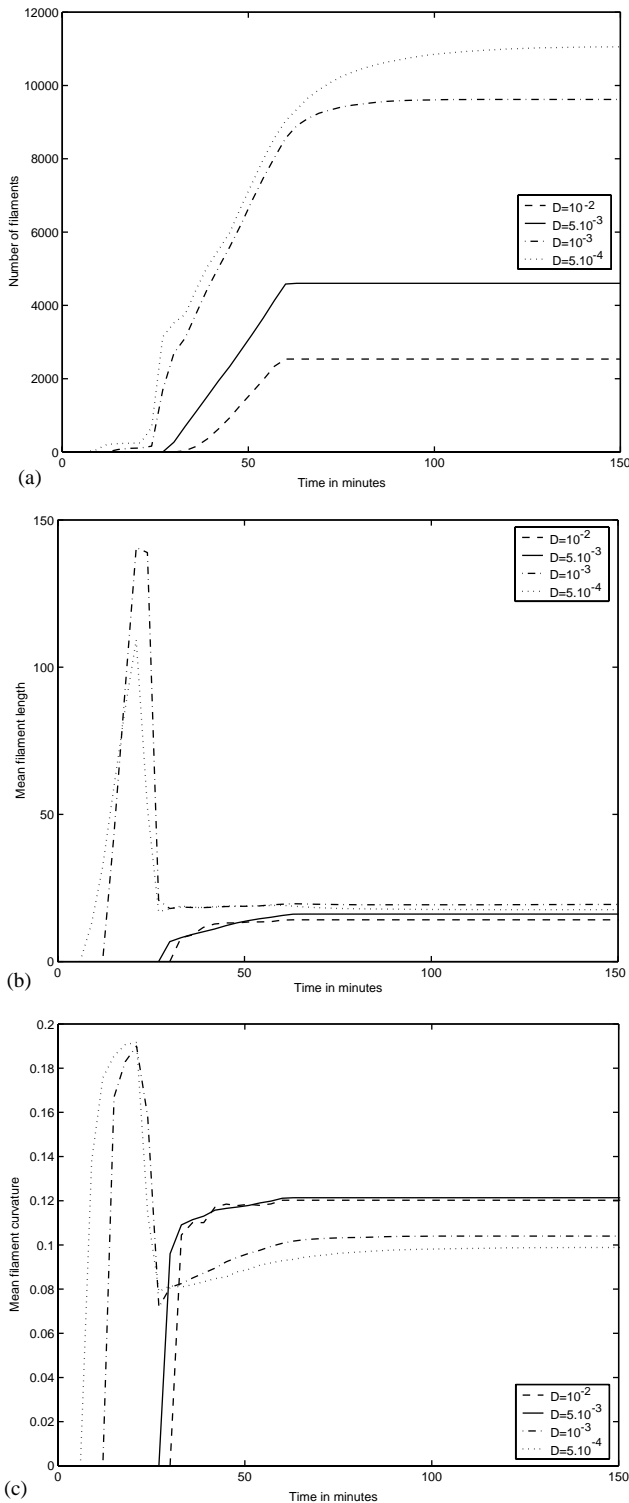


Fig. 9. Influence of the diffusion coefficient: different diffusion coefficients D with a nucleation in perinuclear region and for a stochastic term intensity $\|v\| = 0.25$. (a) represents the evolution with time of the number of filaments constituting the network until the stabilization of building up. (b) depicts the variation through time of the mean filament length until stabilization. (c) describes the changes with time of the mean filament curvature until stabilization.

The function $p(\cdot)$ acts on the instant of nucleation and on the number of filaments. When starting in the perinuclear region, nucleation starts 6 min faster than when it starts in the cortex (Fig. 10). Also, the number of filaments is smaller for a perinuclear nucleation than for a cortex nucleation (Fig. 10(a)). Whatever the nucleation regions, the building up process stabilizes after the same length of time. Thus the filament nucleation influences the network density but plays no role in the filament morphology.

4.3. Influence of the stochastic term $\|v\|$

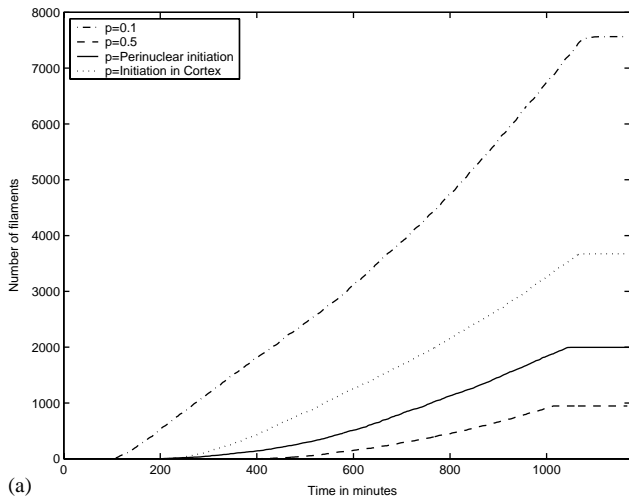
A small stochastic term ($\|v\| = 5 \times 10^{-3}$) induces the nucleation of numerous filaments (7190 filaments against 1972 for $\|v\| = 0.25$, Fig. 11(b)) which grow briefly, reaching a very short mean length (1.29 ± 0.75 , Fig. 11(b)), and adopt very curved shapes similar to a loop (Fig. 11(c)). By increasing the stochastic term, the number of filaments decreases and the mean length of filaments increases.

As the stochastic term increases, the number of filaments is mostly unaffected (Fig. 11(a)). On the other hand, its magnitude strongly affects the mean filament length: for example, the mean length is 14.32 ± 19.02 for a magnitude $\|v\| = 0.25$, but increases to 57.64 ± 62.99 for $\|v\| = 0.1$ (Fig. 11(b)). A weak perturbation allows one to obtain longer filaments exhibiting a quasi rectilinear behavior (Fig. 11(c)): the larger the stochastic term magnitude, the shorter and wavier the filaments. As expected by the Boltzmann theory, at high temperatures, i.e. at high values of $\|v\|$, the filaments become more contorted (Boal, 2002). Thus, the morphology of filaments is more affected by the magnitude of the stochastic term than is the network density.

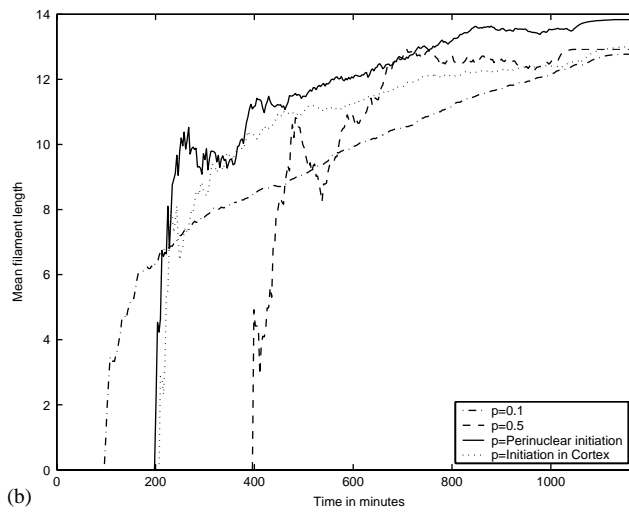
5. Discussion

The model we propose in this paper suggests a new description of the cytoskeleton organization assuming that its function implies its structure. Our working hypothesis, then, is that the guideline of the IF organization is the extracellular mechanical environment, and we use as an underlying hypothesis a regulation of protein synthesis by the mechanical conditions. Mechanically regulated protein synthesis is used to implicitly describe the mechanical environment and its immediate effects on the intracellular domain. The cell then responds to the mechanical environment by aggregating IFs from concentration fields of the soluble pool.

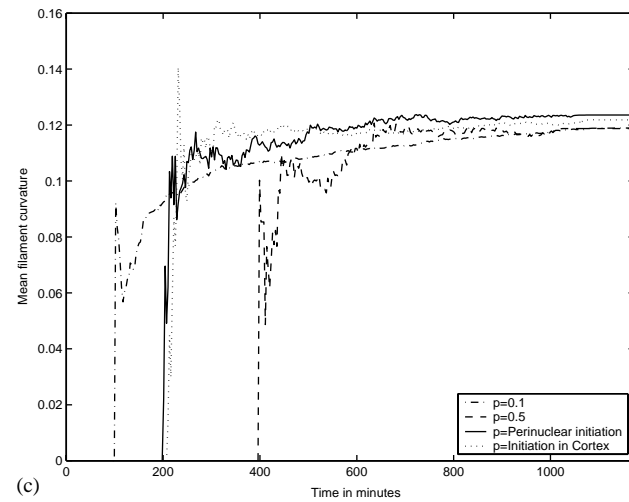
So far, we have successfully reproduced the building up of a network of filaments linking the cell membrane at the anchorage regions to the nucleus envelope (Figs. 6–8) as a result of two basic mechanisms: the



(a)

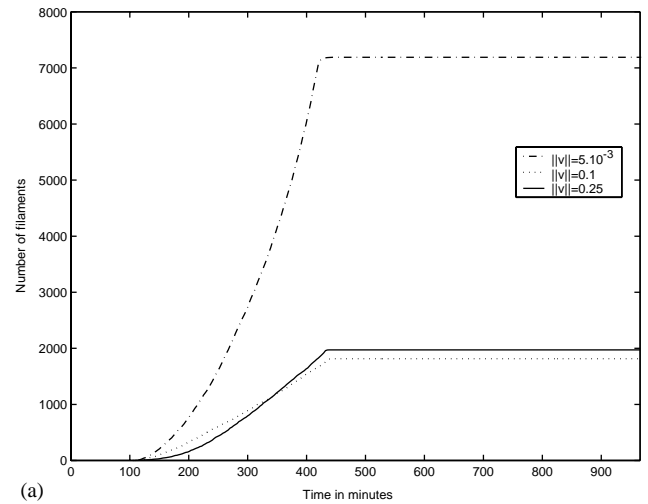


(b)

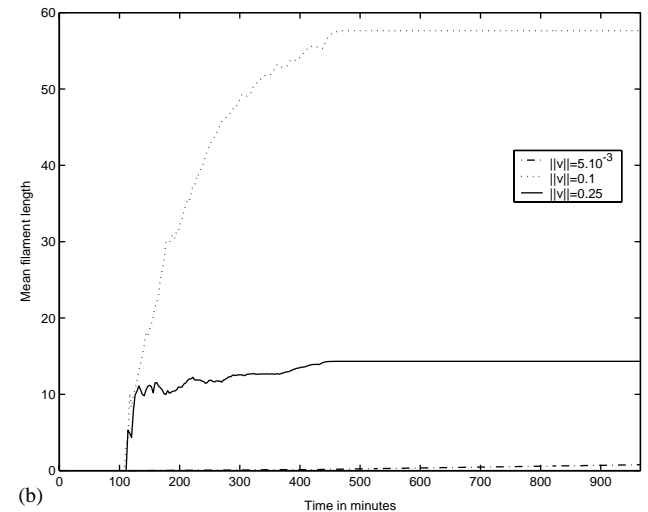


(c)

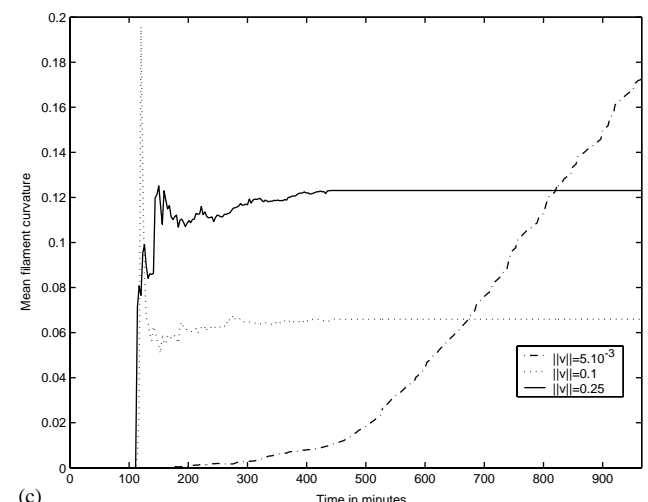
Fig. 10. Influence of the nucleation regions: different nucleation regions (different $p(\cdot)$) for the same diffusion coefficient $D = 5 \times 10^{-4} \mu\text{m}^2 \text{s}^{-1}$ and the same stochastic term intensity $\|v\| = 0.25$. (a) represents the evolution of the number of filaments until stabilization. (b) depicts the variation of the mean filament length until stabilization. (c) describes the changes of the mean filament curvature until stabilization.



(a)



(b)



(c)

Fig. 11. Influence of the stochastic term v : different intensities $\|v\|$ for the same diffusion coefficient $D = 10^{-3} \mu\text{m}^2 \text{s}^{-1}$ and with a nucleation in the perinuclear region. (a) represents the evolution of the number of filaments until stabilization. (b) depicts the variation of the mean filament length until stabilization. (c) describes the changes of the mean filament curvature until stabilization.

diffusion of building blocks within the cytoplasm, on the one hand, and the formation of filaments by an aggregation process of building blocks on the other. According to the intracytoplasmic locations, the mesh is more or less dense: there is an increase of mesh density in the perinuclear region and in the anchorage regions. Qualitatively, the results are in agreement with many observations (Portet et al., 1999; Vassy et al., 2001). The architecture of the *IF* network is dependent on and is induced by the environmental mechanical conditions.

Furthermore, we observe that some model parameters influence the network architecture and the filament morphology. As expected, the regions chosen for nucleation have an effect on the network architecture, mainly on the onset of the building up process as well as on the number of initiated filaments, while, on the other hand, they do not influence the filament morphology. A slow diffusion or a negligible stochastic term also affects the network architecture, leading to a denser network (large number of filaments). The mean filament length is the feature having the largest variability. It is mainly influenced by the magnitude of the stochastic term. Generally, the longer the filaments, the more rectilinear the filament. The diffusion and the stochastic term mainly modulate the morphology of filaments. Filaments adopt a wavier behavior for large stochastic term magnitudes (i.e. at high temperatures) or for diffusion coefficients larger than $D^* = 10^{-3} \mu\text{m}^2 \text{s}^{-1}$. Extensively, according to whether the diffusion coefficient value is lower or bigger than D^* , we observe different behaviors in the simulations. The value D^* separates two qualitatively different behaviors, suggesting that a diffusion coefficient value for the *CK* tetramers lower than D^* could be non-relevant.

The results obtained so far are all but quantitative. It is desirable to work towards obtaining further quantitative results in order to allow for comparison with experimental biological data. Conceptually, the model we proposed here is far too complicated to allow mathematical analysis; it would be desirable to derive a simplified, analytically tractable version. In further work with the proposed mathematical model, we will design a reaction–diffusion model which will allow for easier qualitative study.

In our model, we assume the existence of cohesion forces preserving nuclear integrity. How nuclear integrity is preserved is not yet clearly understood. Some authors suggest a prominent role of *IF* networks (Sarria et al., 1994). In order to account for this phenomenon in the context of the model, a centripetal field of cohesion forces, acting at the perinuclear region, is hypothesized.

Another important process needing a more thorough consideration is the diffusion through the cytoplasm: it could in fact be better modeled as a percolation process (a diffusion driven through a network or a diffusion through a porous medium) or as an active and directed

transport along the *MF* or *MT* networks. The formalism of Eq. (14) governing the soluble pool dynamics is close to the model designed in Robert et al. (1990) for *MT* formation. These authors proposed an equation for the tubulin monomer concentration dynamics which includes a diffusion and a consumption term. We suppose in our model that the diffusion coefficient remains constant. However, the increase in soluble pool concentration and the creation of *CK* network in the cytoplasm would rather imply a rise of the cytoplasm viscosity. Thus, the diffusion coefficient should be a function of the state of the system.

In summary, we assume that cells sense mechanical forces that are transduced by protein synthesis (biochemical signal), and respond by building the *IF* network. We consider the three steps of mechanosensing: perception, transduction and response. Our model can allow a preliminary validation of the hypothesis that was proposed in previous works dealing with *IF* network architecture characterization (see, e.g. Portet et al., 1999; Vassy et al., 2001), namely, that the *IF* network is involved in a mechanotransduction by structural pathways (mechanical signals originating in the extracellular environment are translated into biological signals via (re)organization of the structures).

Acknowledgements

We thank Jack Tuszynski of the University of Alberta (Edmonton, Canada) for helpful discussions during the revision of this work. The authors acknowledge funding from CNES Grant 793/00/CNES/8092 and a grant from A.R.C. Some revisions were carried out while the two first authors were visiting Rice University (Houston, Texas). The authors thank the referees for helpful suggestions.

Appendix A. Simulation model

A.1. Dimensionless model

In the model (Eqs. (14) and (15)), the time and length scales are rescaled as follows:

$$\tilde{x} = \frac{x}{l}, \quad \tilde{y} = \frac{y}{l}, \quad \tilde{z} = \frac{z}{l}, \quad \tilde{t} = \frac{D}{l^2}t,$$

where $l = \sqrt[3]{|\Omega|}$. For convenience, we introduce the parameter, $\varpi = \frac{l}{D}$, and we define $F(\cdot)$ such that it is equal to $F(X, t) = \mathcal{F}(X, t) + \sigma_{\min} \mathbb{1}_{\rho(t) \cup \mathcal{B}(t)}(X)$. The model then is rescaled as follows (omitting the tildes):

$$\frac{\partial C(X, t)}{\partial t} = (\Delta_X C)(X, t) + \varpi F(X, t),$$

$$\frac{dX_\beta(t)}{dt} = \begin{cases} \mathcal{E}(X_\beta(t), t) \left[\frac{(\nabla_X C)(X_\beta(t), t) + \|(\nabla_X C)(X_\beta(t), t)\|v}{\|(\nabla_X C)(X_\beta(t), t)\| + \varepsilon} \right. \\ \left. + \frac{\int_{d_i(\beta)}^t |\kappa(X_\beta(u))| du}{t - d_i(\beta)} \frac{X'_\beta(t_-)}{\|X'_\beta(t_-)\| + \varepsilon} \right] & \forall \beta \in \mathcal{I}(t) \setminus \mathcal{I}_b(t), \\ 0 & \forall \beta \in \mathcal{I}_b(t). \end{cases} \quad (\text{A.1})$$

A.2. Discretization of spatial and temporal domains

The dimensionless cell domain is the unit cube $\Omega = [0, 1] \times [0, 1] \times [0, 1]$. The numerical simulations are carried out in a cubic discrete grid, in the xyz -space (spatial coordinates), that covers Ω . The grid is formed of a set of lines parallel to the x -, y - and z -axis whose intersections define the mesh points. The spacing between two adjacent mesh points in the x -direction (resp. y -direction, resp. z -direction) is uniform, and given by Δx (resp. Δy , resp. Δz). It is assumed that the cell is an isotropic environment, that is to say, the diffusion process takes place in the same way in all directions and moreover $\Delta x = \Delta y = \Delta z = \delta$. The grid spacing δ is correlated with the size of simulations $I \times I \times I$, where $I \in \mathbb{N}$ represents the number of mesh points by lines parallel to the x -direction, $\delta = 1/(I - 1)$. Then the mesh points of the grid are defined as follows: $(x_i, y_j, z_k) = (i\delta, j\delta, k\delta)$ with $i, j, k = 0, 1, \dots, I$.

The dimensionless temporal domain is also subdivided into $N \in \mathbb{N}$ time units such that $(N - 1) \times \Delta t = T_{max}$. The temporal step Δt is defined according to the stability conditions deduced from the approximation of the solution of the diffusion equation.

Each mesh point of the grid is characterized as belonging to a specific cell compartment according to the topology defined in Table 1. Thus, each mesh point is defined as a nuclear point, a nuclear envelope point, a perinuclear point, a cytoplasmic point, a cell membrane point, a desmosome point or a hemidesmosome point (Fig. 12).

A.3. Discretized model

The numerical solution of the first equation of the dimensionless model (A.1) is computed, at transporter mesh points, using the Euler explicit scheme (forward difference in time and central difference in space)

$$C_{i,j,k}^{n+1} = C_{i,j,k}^n + \Delta t \left(\frac{C_{i+1,j,k}^n - 2C_{i,j,k}^n + C_{i-1,j,k}^n}{\delta^2} + \frac{C_{i,j+1,k}^n - 2C_{i,j,k}^n + C_{i,j-1,k}^n}{\delta^2} + \frac{C_{i,j,k+1}^n - 2C_{i,j,k}^n + C_{i,j,k-1}^n}{\delta^2} \right) + \Delta t \varpi F_{i,j,k}^n, \quad (\text{A.2})$$

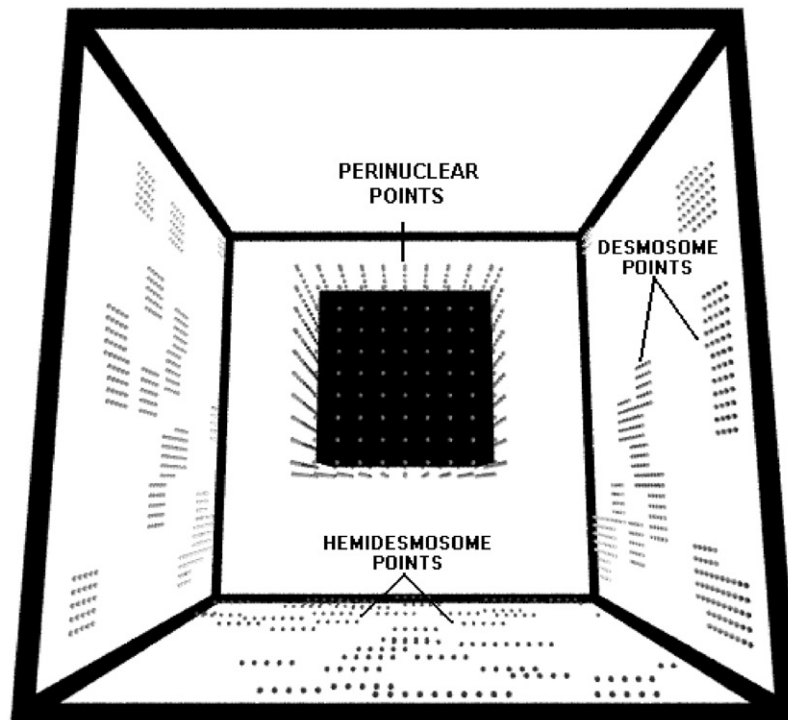


Fig. 12. Discrete epithelial cell. The black cube in the center of the domain is the nucleus. The gray points, enclosing the nucleus, are the perinuclear mesh points. On the lateral faces, the gray points are the desmosome mesh points, that form the different desmosome plaques. On the basal face, the gray points describe the hemidesmosome mesh points. The black regions, i.e. the edges of the cell and the nucleus, do not belong to the working domain. The other mesh points of the domain are not shown in the figure.

where the mesh function C_{ijk}^n represents the approximated solution of $C(x, y, z, t)$, at grid point (x_i, y_j, z_k, t_n) . The initial condition (8) is approximated by $C_{i,j,k}^0 = 0$ for all i, j and k . At the cytoplasm boundary points, the boundary conditions, defined by Eq. (9), modify the computation of the numerical solution. For the conditions on the outer boundary $\partial\Omega$ of the cytoplasm domain, artificial points are added to the cytoplasm domain, $x_{-1} = 0 - \delta$ and $x_{I+1} = 1 + \delta$ in the x -direction, $y_{-1} = 0 - \delta$ and $y_{I+1} = 1 + \delta$ in the y -direction, and $z_{-1} = 0 - \delta$ and $z_{I+1} = 1 + \delta$ in the z -direction. Then the Neumann boundary condition is approximated as follows:

$$\frac{\partial C}{\partial n}|_{\partial\Omega} = 0 \Leftrightarrow \begin{cases} -\frac{\partial C}{\partial x}|_{x=x_0} \simeq -\frac{C_{1,j,k}^n - C_{-1,j,k}^n}{2\delta} = 0, \\ \frac{\partial C}{\partial x}|_{x=x_I} \simeq \frac{C_{I+1,j,k}^n - C_{I-1,j,k}^n}{2\delta} = 0, \\ -\frac{\partial C}{\partial y}|_{y=y_0} \simeq -\frac{C_{i,1,k}^n - C_{i,-1,k}^n}{2\delta} = 0, \\ \frac{\partial C}{\partial y}|_{y=y_I} \simeq \frac{C_{i,I+1,k}^n - C_{i,I-1,k}^n}{2\delta} = 0, \\ -\frac{\partial C}{\partial z}|_{z=z_0} \simeq -\frac{C_{i,j,1}^n - C_{i,j,-1}^n}{2\delta} = 0, \\ \frac{\partial C}{\partial z}|_{z=z_I} \simeq \frac{C_{i,j,I+1}^n - C_{i,j,I-1}^n}{2\delta} = 0. \end{cases} \quad (\text{A.3})$$

The normal derivatives on the faces perpendicular to the x -axis (resp. y -axis, resp. z -axis) give the condition $C_{i-1,j,k}^n = C_{i+1,j,k}^n$ (resp. $C_{i,j-1,k}^n = C_{i,j+1,k}^n$, resp. $C_{i,j,k-1}^n = C_{i,j,k+1}^n$), at points of spatial coordinate x_0 and x_I (resp. y_0 and y_I , resp. z_0 and z_I), that will be used in the explicit scheme (Strikwerda, 1989). We proceed in the same way for the approximation of Neumann boundary conditions applying at mesh points of inner boundary ∂N of the cytoplasm domain.

The Courant condition is used as a stability criterion for the numerical solutions and allows the determination of a maximal size for the time step Δt : $\Delta t \leq \delta^2/6$. Moreover, the time step Δt must be higher than the time scale of lateral assembly of tetramers into *ULF* (a process not described in the model since it is much faster than the time step). For all mesh points of the cytoplasm domain, the diffusion process is computed by using the explicit scheme iterated with the method of Liebmann (Harris and Stocker, 1998).

The mesh function $F_{i,j,k}^n$ is an approximation of the function $F(X, t) = \mathcal{F}(X, t) + \sigma_{min} \mathbb{1}_{\rho(t) \cup \mathcal{B}(t)}(X)$ at (x_i, y_j, z_k, t_n) . For all points (x_i, y_j, z_k, t_n) , the quantity of soluble pool secreted in the unit volume is evaluated through the synthesis function $\mathcal{F}_{i,j,k}^n$. The degradation of soluble pool at point (x_i, y_j, z_k, t_n) depends on the nucleation or the filament growth at this point. The occurrence of one of these two events, at point

(x_i, y_j, z_k, t_n) , implies that a soluble pool density equal to σ_{min} is consumed.

For all points (x_i, y_j, z_k, t_n) , the nucleation susceptibility is calculated using Eq. (10) and is compared to the threshold function $p(\cdot)$. $p(\cdot)$ can be a constant function such that $\forall(x_i, y_j, z_k, t_n), p(\cdot) = b$ with $b \in (0, 1]$. It can also be a space-dependent function (Fig. 4), defined as a function of the distance from a site to the nucleus such that $\forall X = (x_i, y_j, z_k), \forall t_n, p_{i,j,k} = ad(X, N) + b$ with $a \leq 1/\max_{Y \in \Omega} [d(Y, N)]$ and $0 \leq b \leq 1$, where $d(\cdot)$ is a discrete distance. When the coefficient a is strictly positive, the nucleation is favored in the sites surrounding the nucleus. On the other hand, a coefficient a strictly negative favors the nucleation in the sites of the cell cortex.

All points (x_i, y_j, z_k, t_n) verifying Eq. (11) become nucleation centers and filament points: the mesh point $(x_i, y_j, z_k) = \beta$, at time t_n , is the nucleation center. As does the diffusion process, the nucleation and growth of filaments take place at the mesh points of the grid: a trajectory (a filament) is a discrete path in the grid. Contrary to the environmental processes, that run on a 6-connectivity grid, the processes of building up of filaments use a grid with a 26-connectivity: $N_{26}(p) = \{p' \in \Omega \mid d(p, p') \leq \sqrt{3}\delta\}$.

For all iterations $n\Delta t$, at all filament tips not having reached the domain boundary, the growing trajectory is calculated using Eq. (15). If the soluble pool mean density around the tip of filament is lower than σ_{min} , no filament growth can take place. For all tips $X_\beta(t) = (x_i^\beta, y_j^\beta, z_k^\beta, t_n)$ of growing filaments, the approximation of the concentration local gradient is accomplished by a centered difference.

The three-dimensional random vector v is drawn under the following conditions: the components v_x, v_y and v_z are independent, uniformly distributed random variables, with values in $[-\sqrt{3}\delta, \sqrt{3}\delta]$. The vector v is then normalized and multiplied by a scalar less than $\frac{1}{4}$. Therefore, we have $\|v\| \leq \frac{1}{4}$. This value was arbitrarily chosen so that the magnitude of the stochastic term stays within admissible bounds, avoiding the case where stochasticity becomes the driving component of the dynamics.

The tangent vector at a given filament tip is approximated by the forward difference at the next to the last filament point, starting from the third iteration after the instant of nucleation (for example, if the filament starts at time t_n^β , the computation of the tangent vector starts at t_{n+2}^β).

The curvature along the filament $X_\beta(\cdot)$ is calculated, at each tip $(x_i^\beta, y_j^\beta, z_k^\beta, t_n)$, as follows:

$$|\kappa(X_\beta(t))| = \sqrt{\frac{X'_\beta(t)^2 X''_\beta(t)^2 - (X'_\beta(t) X''_\beta(t))^2}{X'_\beta(t)^6}} \quad (\text{A.4})$$

that is estimated with second-order central and forward differences at filament point $(x_i^\beta, y_j^\beta, z_k^\beta, t_{n-1})$.

At iterations t_n^β , t_{n+1}^β and t_{n+2}^β , $\kappa(X_\beta(t))$ is supposed to be equal to zero.

References

- Boal, D., 2002. *Mechanics of the Cell*. Cambridge University Press, Cambridge.
- Bolterauer, H., Limbach, H.-J., Tuszynski, J., 1996. From stochastic to coherent assembly of microtubules: Models and new results. *Bioelectrochem. Bioenergetics* 41, 71–76.
- Bray, D., 1992. *Cell Movements*. Garland Publishing, INC, New York.
- Chicurel, M., Singer, R., Meyer, C., Ingber, D., 1998. Recruitment of mRNA and ribosomes to focal adhesions triggered by integrin binding and mechanical tension. *Nature* 392, 730–733.
- Chou, Y., Goldman, R., 2000. Intermediate filaments on the move. *J. Cell Biol.* 150, 101–105.
- Chou, C., Riopel, C., Rott, L., Omary, M., 1993. A significant soluble keratin fraction in 'simple' epithelial cells. Lack of an apparent phosphorylation and glycosylation role in keratin solubility. *J. Cell Sci.* 105, 433–444.
- Civelekoglu, G., Edelstein-Keshet, L., 1994. Modelling the dynamics of F-actin in the cell. *Bull. Math. Biol.* 56, 587–616.
- Coulombe, P., Bousquet, O., Ma, L., Yamada, S., Wirtz, D., 2000. The 'ins' and 'outs' of intermediate filament organization. *Trends Cell Biol.* 10, 420–428.
- Dallon, J., Sherratt, J.A., 2000. A mathematical model for spatially varying extracellular matrix alignment. *SIAM J. Appl. Math.* 61, 506–527.
- Dallon, J., Sherratt, J., Maini, P., 1999. Mathematical modelling of extracellular matrix dynamics using discrete cells: Fibers orientation and tissue regeneration. *J. Theor. Biol.* 199, 449–471.
- Dufort, P.A., Lumsden, C., 1993. Cellular automaton model of the actin cytoskeleton. *Cell Motility Cytoskeleton* 25, 87–104.
- Eckes, B., Dogic, D., Colucci-Guyon, E., Wang, N., Maniotis, A., Ingber, D., Merckling, A., Langa, M., Aumailley, F., Delouée, A., Kotliansky, V., Babinet, C., Krieg, T., 1998. Impaired mechanical stability, migration and contractile capacity in vimentin-deficient fibroblast. *J. Cell Sci.* 111, 1897–1907.
- Edelstein-Keshet, L., Ermentrout, G., 2000. Models for spatial polymerization dynamics of rod-like polymers. *J. Math. Biol.* 40, 64–96.
- Geisler, N., Schunemann, J., Weber, K., Haner, M., Aebi, U., 1998. Assembly and architecture of invertebrate cytoplasmic intermediate filaments reconcile features of vertebrate cytoplasmic and nuclear lamin-type intermediate filaments. *J. Mol. Biol.* 282, 601–617.
- Goldman, R., Khuon, S., Chou, Y., Opal, P., Steinert, P., 1996. The function of intermediate filaments in cell shape and cytoskeletal integrity. *J. Cell Biol.* 134, 971–983.
- Harris, J., Stocker, H., 1998. *Handbook of Mathematics and Computational Science*. Springer, Berlin.
- Hatzfeld, M., Burba, M., 1994. Function of type I and type II keratin head domains: their role in dimer, tetramer and filament formation. *J. Cell Sci.* 107, 1959–1972.
- Herrmann, H., Aebi, U., 2000. Intermediate filaments and their associates: multi-talented structural elements specifying cyto-architecture and cytodynamics. *Curr. Opin. Cell Biol.* 12, 79–90.
- Howard, J., 2001. *Mechanics of Motor Proteins and the Cytoskeleton*. Sinauer Associated Inc.
- Ingber, D., 1993. Cellular tensegrity: defining new rules of biological design that govern the cytoskeleton. *J. Cell Sci.* 104, 613–627.
- Ingber, D., 1997. Tensegrity: the architectural basis of cellular mechanotransduction. *Annu. Rev. Physiol.* 59, 575–599.
- Janosi, I., Chretien, D., Flyvbjerg, H., 1998. Modeling elastic properties of microtubule tips and walls. *Eur. Biophys. J.* 27, 501–513.
- Jansen, R., 1999. RNA-cytoskeletal associations. *FASEB J.* 13, 455–466.
- Ma, L., Xu, J., Coulombe, P., Wirtz, D., 1999. Keratin filament suspensions show unique micromechanical properties. *J. Biol. Chem.* 274, 19145–19151.
- McGrath, J., Tardy, Y., Dewey, C., Meister, J., Hartwig, J., 1998. Simultaneous measurements of actin filament turnover, filament fraction, and monomer diffusion in endothelial cells. *Biophys. J.* 75, 2070–2078.
- Mech, R., Prusinkiewicz, P., 1996. Visual models of plants interacting with their environment. In: *Proceedings of SIGGRAPH 96*, New Orleans, Louisiana, August 4–9, 1996, In *Computer Graphics. ACM SIGGRAPH*, New York.
- Mogilner, A., Edelstein-Keshet, L., 1996. Spatio-angular order in populations of self-aligning objects: formation of oriented patches. *Physica D* 89, 346–367.
- Mogilner, A., Oster, G., 1999. The polymerization ratchet model explains the force-velocity relation for growing microtubules. *Eur. Biophys. J.* 28, 235–242.
- Portet, S., Vassy, J., Beil, M., Millot, G., Hebbache, A., Rigaut, J., Schoevaert, D., 1999. Quantitative analysis of cytokeratin network topology in the MCF7 cell line. *Cytometry* 35, 203–213.
- Potard, U., Butler, J.P., Wang, N., 1997. Cytoskeletal mechanics in confluent epithelial cells probed through integrins and E-cadherins. *AJP—Cell Physiol.* 272, C1654–C1663.
- Robert, C., Bouchiba, M., Robert, R., Margolis, R., Job, D., 1990. Self organization of the microtubule network. A diffusion based model. *Biol. Cell* 68, 177–181.
- Sarria, A., Lieber, J., Nordeen, S., Evans, R., 1994. The presence or absence of a vimentin-type intermediate filament network affects the shape of the nucleus in human SW-13 cells. *J. Cell Sci.* 107, 1593–1607.
- Sept, D., Limbach, H., Bolterauer, H., Tuszynski, J., 1999. A chemical kinetics model for microtubule oscillations. *J. Theor. Biol.* 197, 77–88.
- Sherratt, J.A., Lewis, J., 1993. Stress-induced alignment of actin filaments and the mechanics of cytogel. *Bull. Math. Biol.* 55, 637–654.
- Smith, E., Fuchs, E., 1998. Defining the interactions between intermediate filaments and desmosomes. *J. Cell Biol.* 141, 1229–1241.
- Sonnenberg, A., de Melker, A., Martinez de Velasco, A., Janssen, H., Calafat, J., Niessen, C., 1993. Formation of hemidesmosomes in cells of a transformed murine mammary tumor cell line and mechanisms involved in adherence of these cells to laminin and kalinin. *J. Cell Sci.* 106, 1083–1102.
- Spiros, A., Edelstein-Keshet, L., 1998. Testing a model for the dynamics of actin structures with biological parameter values. *Bull. Math. Biol.* 60, 275–305.
- Stokes, C., Lauffenburger, D., 1991. Analysis of the roles of microvessel endothelial cell random motility and chemotaxis in angiogenesis. *J. Theor. Biol.* 152, 377–403.
- Strikwerda, J., 1989. *Finite Difference Schemes and Partial Differential Equations*. Wadsworth and Brooks, California.
- Suciu, A., Civelekoglu, G., Tardy, Y., Meister, J., 1997. Model for the alignment of actin filaments in endothelial cells subjected to fluid shear stress. *Bull. Math. Biol.* 59, 1029–1046.
- Thoumine, O., Ziegler, T., Girard, P., Nerem, R., 1995. Elongation of confluent endothelial cells in culture: The importance of fields of force in the associated alterations of their cytoskeletal structure. *Exp. Cell Res.* 219, 427–441.
- Vaario, J., Onitsuka, A., Shimohara, K., 1997. Formation of neural structures. In: *Husbands, P., Harvey, I. (Eds.), The Proceedings of the Fourth European Conference on Artificial Life*. The MIT Press, Boston.

- Vassy, J., Portet, S., Beil, M., Millot, G., Fauvel-Lafeve, F., Karniguian, A., Gasset, G., Irinopoulou, T., Calvo, F., Rigaut, J., Schoevaert, D., 2001. The effect of weightlessness on cytoskeleton architecture and proliferation of human breast cancer cell line MCF-7. *FASEB J. Express* 15, 1104–1106.
- Wang, J., 2000. Substrate deformation determines actin cytoskeleton reorganization: a mathematical modeling and experimental study. *J. Theor. Biol.* 202, 33–41.
- Wang, N., Ingber, D., 1994. Control of cytoskeletal mechanics by extracellular matrix, cell shape, and mechanical tension. *Biophys. J.* 66, 2181–2189.
- Wang, N., Stamenovic, D., 2000. Contribution of intermediate filaments to cell stiffness, stiffening and growth. *Am. J. Physiol. Cell Physiol.* 279, 188–194.
- Wendling, S., Oddou, C., Isabey, D., 1999. Stiffening response of a cellular tensegrity model. *J. Theor. Biol.* 196, 309–325.